

Discontinuous Displacement at Solvent–Immobile Hydrocarbon Interfaces

by

Haoxiang Wang

A thesis submitted in partial fulfillment of the requirements for the degree of

Master of Science

in

Petroleum Engineering

Department of Civil and Environmental Engineering
University of Alberta

© Haoxiang Wang, 2020

ABSTRACT

Concerns over the environmental impacts of thermal production methods for bitumen and heavy oil have led to the exploration of alternative technologies including solvent-assisted production methods. While solvent-assisted production methods have been studied extensively, apparent diffusion rates of the penetrating solvent one to two orders of magnitude greater than those predicted from the Fickian diffusion are required to match production histories. “Surface renewal” and “sloughing” mechanisms have been suggested to explain such abnormally high solvent penetration rates during production but have not been observed directly or included in process models.

In this work, high-resolution X-ray videography is employed to investigate solvent penetration at interfaces between a model solvent (n-pentane) and a model immobile reservoir fluid (octacosane) over time and observe “surface renewal” and “sloughing” directly for the first time. Solvent and wax are sealed in shell glass vials in contact with each other creating solvent-wax interfaces. Various solvent-wax interfaces, including the horizontal interface with the wax below, horizontal interface with the solvent below, as well as the vertical interface, are studied. The interface progressions are analyzed by using the software ImageJ™ to track intensity changes over time.

The experimental results show that for horizontal interfaces (octacosane below), interface displacement arises solely from diffusion and rates of displacement are slow ($\sim 10^{-2}$ $\mu\text{m/s}$). For vertical pentane-octacosane interfaces and horizontal pentane-octacosane interfaces (pentane below) steady displacement rates, an order of magnitude greater than for diffusion alone, are

punctuated by rapid detachments of $\sim 30 \mu\text{m}$ layers of octacosane-enriched liquid from the interface at $\sim 150 \text{ s}$ intervals. For vertical interfaces, that dominate production processes especially in thin reservoirs, average interface displacement rates approaching $10^0 \mu\text{m/s}$ are realized.

These findings highlight the impact of interface orientation on interface displacement rate. They also provide quantitative insights into the kinetics of solvent-assisted bitumen and heavy oil production processes in high-permeability reservoirs, needed as inputs for modeling “surface renewal” and “sloughing” mechanisms directly in these processes.

PREFACE

The research work presented in this dissertation has been submitted as a journal paper for publication—"Wang, H., Shaw, J.M., and Jin, Z., Discontinuous Displacement at Solvent-Immobilized Hydrocarbon Interfaces, submitted to *Energy & Fuels*". I am the first author of this manuscript. Professor John M. Shaw and Professor Zhehui Jin extensively helped with all aspects of the research work.

ACKNOWLEDGEMENTS

My utmost gratitude to my supervisor, Dr. Zhehui Jin, whose serious attitude towards research set an example to me of how to become a qualified researcher. His constant trust and guidance, even at the toughest moment during my study, helped me to complete this degree.

My sincere appreciation to Dr. John M. Shaw, who provided me with so much advice and help towards my experimental works and manuscript. I am also grateful to Dr. Lijun Deng and Dr. Juliana Leung for being my examination committee members and their generous comments. It is my pleasure to acknowledge Dr. Nobuo Maeda for his kind input regarding my research project.

I would like to thank Dr. Na Jia, who guided me in doing experiments during my undergraduate study. Her patience and kindness lead me to continue pursuing this degree. Many thanks to my parents and grandparents for their constant love to me. I would also wish to thank all my friends. This journey would be much harder without their companionship and support.

I greatly acknowledge a Discovery Grant from Natural Sciences and Engineering Research Council of Canada to Z. Jin. I am also thankful to the University of Alberta Future Energy Systems (FES) and the Canada First Research Excellence Fund (CFREF) for providing financial support for the project, and to the NSERC Industrial Research Chair Program for providing the facility.

DEDICATION

This dissertation is dedicated to my Mother, Mrs. Hongxia Tian,
for her love, support, and guidance throughout my life.

TABLE OF CONTENTS

ABSTRACT	ii
PREFACE	iv
ACKNOWLEDGEMENTS	v
DEDICATION	vi
LIST OF TABLES	x
LIST OF FIGURES	xi
NOMENCLATURE	xiv
CHAPTER 1 INTRODUCTION	1
1.1 Research Background.....	1
1.2 Problem Statement	3
1.3 Research Objectives	4
1.4 Thesis Outline	5
CHAPTER 2 LITERATURE REVIEW	6
2.1 Heavy Oil and Bitumen Resources	6
2.2 The Thermal Recovery Methods.....	8
2.3 The Solvent-Assisted Recovery Methods	8
2.3.1 Solvent Chamber Evolution.....	9

2.4 Mathematical Model of the Solvent Recovery Method	10
2.5 Experimental Study of the VAPEX Model	14
2.6 Hypothesis of the “Sloughing” Phenomenon.....	16
2.7 Solvent Diffusivity in Bitumen	19
CHAPTER 3 EXPERIMENT SECTION.....	21
3.1 Methodology	21
3.2 Experimental Setup	21
3.3 Experimental Procedure	24
3.3.1 Sample Preparation.....	24
CHAPTER 4 RESULTS AND DISCUSSION.....	26
4.1 Overview	26
4.2 Air + Octacosane System	26
4.3 Horizontal Interface with Octacosane Below.....	30
4.4 Horizontal Interface with Pentane Below	35
4.5 Vertical Interface.....	40
4.6 Summary	47
4.7 Quantifying “Surface Renewal” or “Sloughing” Effects in Production Models	48
CHAPTER 5 CONCLUSIONS AND RECOMMENDATIONS	51
5.1 Conclusions	51
5.2 Recommendations	52

BIBLIOGRAPHY.....	54
APPENDIX A: “EFFECTIVE DIFFUSIVITY” CALCULATION BASED ON DAS AND BUTLER’S EXPERIMENTAL RESULTS.....	61
APPENDIX B: FLOWCHART OF EXPERIMENTAL PROCEDURES	65
APPENDIX C: EXPERIMENTAL DATA OF THE VERTICAL PENTANE-OCTACOSANE INTERFACE SCENARIO.....	66

LIST OF TABLES

Table 2-1. Characteristics of typical Canadian heavy oil reservoirs (Dusseault, 2001; James et al., 2007; Lin, 2014).....	7
Table 2-2. Comparison of predicted and actual bitumen production rates in sand-packed cells (Das and Butler, 1994b)	15
Table 3-1. List of chemicals used in experiments.....	22
Table 4-1. Summary of the interface progress rates	48
Table A-1. List of parameters for calculating butane “effective diffusivity”	63
Table A-2. Summary of variables at different butane volume concentration.....	64
Table C-1. Intensity data from 0 to 100 seconds	66
Table C-2. Interface displacement in 1000 seconds with 10 seconds time intervals.....	74
Table C-3. Interface displacement from 250 to 350 seconds with 0.5 seconds time intervals.....	75

LIST OF FIGURES

Figure 2-1. Major heavy oil reserves in Canada (PetroWiki, 2020).....	7
Figure 2-2. Schematic of the solvent rising, spreading, and falling phases during solvent extraction processes (Lin, 2014)	10
Figure 2-3. Schematic of a Hele-Shaw cell	11
Figure 2-4. Schematic of the diffusion layer of the Butler-Mokry's model (Das and Butler, 1998)	13
Figure 2-5. Periodic asphaltene deposition observed on a Hele-Shaw cell from a VAPEX experiment (Das and Butler, 1998).....	15
Figure 2-6. Mechanisms of sloughing events (Stewart and Shaw, 2018).....	16
Figure 2-7. Energy exchange during drop mobilization. The letter “S” and “B” represent solvent and bitumen phases, respectively.....	18
Figure 2-8. Theoretical comparison of the interface displacement rates between continuous interface advancements and the “sloughing” mechanism.....	18
Figure 2-9. Butane effective diffusivity calculated based on Das and Butler’s experimental results (Das and Butler, 1994b).....	20
Figure 3-1. Schematic representations of the interface orientations and geometries: (a) horizontal interface with octacosane below; (b) horizontal interface with pentane below; (c) vertical interface	22

Figure 3-2. The Schematic of the X-ray system	23
Figure 3-3. Procedures of creating the pentane-octacosane interfaces	25
Figure 4-1. X-ray still image showing a cross-section of a glass vial adjacent to an air-octacosane interface. The area of interest is analyzed to obtain the elevation-averaged intensity profile shown in Figure 4-2.....	28
Figure 4-2. Elevation-averaged intensity profile for the area of interest shown in Figure 4-1. The midpoint of the interface is highlighted in the inset	29
Figure 4-3. Images of the pentane-octacosane system with a horizontal interface (octacosane below): (a) at the initial state and (b) 1 hour later.....	32
Figure 4-4. Intensity profiles of the areas of interest in the pentane-octacosane system in Figure 4-3 with a horizontal interface (octacosane below) at the initial state and 1 hour later	33
Figure 4-5. Interface displacement for the pentane-octacosane system with a horizontal interface (octacosane below).....	34
Figure 4-6. Images of the pentane-octacosane system with a horizontal interface (pentane below): (a) at the initial state and (b) 1 hour later.....	36
Figure 4-7. Intensity profiles of the areas of interest in the pentane-octacosane system in Figure 4-6 with a horizontal interface (pentane below) at the initial state and 1 hour later	37
Figure 4-8. Interface displacement for the pentane-octacosane system with a horizontal interface (pentane below) from 0 to 1000 s	38
Figure 4-9. Interface displacement during the jump event from 520 s to 620 s highlighted with red dashed brackets in Figure 4-8	39

Figure 4-10. Images of the pentane-octacosane system with a vertical interface: (a) at the initial state and (b) 1 hour later 42

Figure 4-11. Intensity profiles of the area of interest in the pentane-octacosane system in Figure 4-10, vertical interface, at the initial state and 1 hour later 43

Figure 4-12. Interface displacement for the pentane-octacosane system with a vertical interface from 0 to 1000 s. The red dashed bracket area highlights the area analyzed in Figure 4-13..... 44

Figure 4-13. Interface displacement during the jump event from 250 s to 350 s highlighted with red dashed brackets in Figure 4-12 45

Figure 4-14. A sudden jump of the pentane-octacosane interface. The black grids represent pentane-heavy-blocks, while the white grids represent octacosane-heavy-blocks..... 46

Figure 4-15. A comparison of predicted production rates using the Butler-Mokrys model and parameterized in this work with measured production rates (Das and Butler, 1994a; Das and Butler, 1994b) 50

NOMENCLATURE

Symbols

ξ	Thickness of solvent-bitumen interface
v	Diluted bitumen drainage rate
U	Solvent-bitumen interface advancing speed
Q	Bitumen production rate
k	Cell permeability
g	Gravitational acceleration
ϕ	Cell porosity
ΔS_o	Change in oil saturation
h	Height of the cell
N_s	Dimensionless number
c_m	Minimum volume concentration of solvent in solvent-bitumen mixture required to mobilize
c_i	Solubility of solvent in bitumen
c_s	Volume fraction of solvent in diluted bitumen
c_B	Volume fraction of bitumen in diluted bitumen
$\Delta\rho$	Density difference between the diluted bitumen and pure solvent
μ	Viscosity of diluted bitumen
D_s	Intrinsic diffusivity of solvent in bitumen

a	Vapex parameter
ΔE	Drop mobilization energy
A	Surface area of a bitumen drop
σ	Interfacial tensions
H	Change of the center of gravity
ρ	Density
V_B	Volume of bitumen drops
$I_{Pentane}$	Average intensity of the pentane phase
$I_{Octacosane}$	Average intensity of the octacosane phase
$I_{Interface}$	Average of solvent and wax phase intensity

Subscripts

1	Oil formation 1
2	Oil formation 2
B	Bitumen
S	Solvent
WS	Between water and solvent
BS	Between bitumen and solvent
WB	Between water and bitumen

Acronyms

SAGD	Steam-assisted gravity drainage
CSS	Cyclic steam stimulation
ISC	<i>In-situ</i> Combustion
GHG	Greenhouse gas
VAPEX	Vapor extraction
IFT	Interfacial tension

CHAPTER 1 INTRODUCTION

1.1 Research Background

With the depletion of conventional light oil reserves, exploitation of heavy oils and bitumen plays an important role in total petroleum supply (Hein, 2017; Nasr and Ayodele, 2006). Canada has abundant heavy oils and bitumen resources. However, they are immobile at their natural state due to extremely high viscosity (Speight, 2014). Additional reservoir stimulations are required to extract crude oils from heavy oil and bitumen reservoirs (Hart, 2014).

Thermal recovery methods inject high-quality steam to conduct heat to heavy crude oils (White and Moss, 1965). One of the most well-known methods is the steam-assisted gravity drainage (SAGD), which applies in many oil sand formations drilled with two parallel horizontal wells (Edmunds and Gittins, 1993). Steam is continuously injected through perforations of the upper horizontal well forming steam chambers that are in contact with cold viscous heavy oils and bitumen at high temperatures. The heated reservoir fluid dramatically reduces its viscosity and flows down to the production well by gravity drainage (Irani and Ghannadi, 2013). Although the application of thermal recovery methods is successful in many projects (Jimenez, 2008), a series of environmental concerns (such as a large amount of water usage, high energy input to generate steam, wastewater disposal, etc.) arise (Swenson et al., 2012). As environmental regulation is tightening, the oil sands industry is facing significant challenges. Its social license is in question, and high capital costs for new projects (Chaar et al., 2015) and depressed oil prices bring more uncertainties to the industry.

Currently, many researchers and oil companies are trying to develop production technologies with significantly lower environmental impacts including solvent-assisted bitumen production methods (Orr, 2009). Solvents, such as propane, butane, and pentane, in liquid or vapor state, are injected alone or co-injected with steam into heavy oil and bitumen formations to reduce petroleum crude viscosity by solvent diffusion (Gates and Chakrabarty, 2006; Nasr et al., 2003; Orr, 2009; Pathak et al., 2011; Pathak et al., 2012). The major advantages of these methods are cutting down the usage of water and energy intensity (Gates, 2010). Solvent extraction methods also eliminate the requirement of large disposal of wastewater. Instead, solvents can be recycled and reused (James et al., 2007). The produced solvent-bitumen mixture is further processed to separate light solvents from the mixture. The separated solvent can be reinjected into the reservoir. Besides, solvent extraction projects have low capital costs as they do not require additional surface facilities to generate steam and handle wastewater (Upreti et al., 2007).

Extensive researches regarding the topic of solvent-assisted production methods have been conducted, including mathematically modelling the production processes (Das and Butler, 1994a; Das and Butler, 1995; Das and Butler, 1994b; Das and Butler, 1996; Das and Butler, 1998). The most well-known production model is the Butler-Mokrys model (Mokrys and Butler, 1993). However, it underestimates bitumen production rates by 3-5 times compared to experimental production data. Besides, experimentally measured solvent-bitumen mutual diffusion coefficients are two to three orders of magnitude lower than the hypothesized apparent diffusivity values required to matching the actual production data (Tharanivasan et al., 2004; Zhang et al., 2007; Zhang and Shaw, 2007). Although with forced convection, mass transfer rates can be up to two orders of magnitude higher than diffusion-based rates (Sadighian et al., 2011), it is impossible to apply shear force at bitumen-solvent interfaces in a porous media.

Das and Butler (Das and Butler, 1998) proposed that “surface renewal” is the reason for enhanced solvent mass transfer rates across solvent-bitumen interfaces. More recently, Stewart and Shaw (Stewart and Shaw, 2018) proposed the “sloughing” mechanism that contributes to accelerated solvent diffusion within a pore. However, none of the proposed mechanisms have been experimentally observed. Therefore, there are needs to understand which mechanisms dictate mass transfer at solvent-bitumen interfaces and investigate the possibility of “surface renewal” and “sloughing” mechanisms.

1.2 Problem Statement

To minimize environmental impact during heavy oils and bitumen production, it is urgent to develop solvent extraction methods with less water usage, energy consumption, and greenhouse gas (GHG) emission. The production rate is one of the most important indicators to evaluate the feasibility of heavy oil and bitumen exploitation projects. However, the current mathematical model cannot precisely predict the actual production rates that are 3-5 times higher than the predicted values (Das and Butler, 1994b). Apparent diffusivities, applied to explain accelerated solvent mass transfer rates, are one to two orders of magnitude greater than the solvent diffusivities based on the Fickian diffusion (Stewart and Shaw, 2018). While an enhanced interfacial mass transfer at bitumen-solvent interfaces is hypothesized to occur during solvent injection into reservoirs, direct measurement of “surface renewal” and “sloughing” phenomena has not been realized. To precisely predict bitumen production rates, it is essential to fully understand the mechanisms involved during the solvent-assisted production processes. Mass transfer of solvent in the solvent-bitumen system has not been fully understood. The solvent-bitumen interface

physical/chemical property change during the solvent mass transfer process needs to be investigated. To unlock the underlying mechanisms of the solvent extraction method, a detailed understanding of the bitumen-solvent interface is imperative.

1.3 Research Objectives

The objective of this work is to investigate the underlying mechanisms of solvent mass transfer during solvent-assisted bitumen production processes. n-Pentane is used as the solvent, while octacosane is used as the surrogate of bitumen. A series of experiments are performed to investigate how pentane-octacosane interfaces progress with different interface orientations by using an X-ray videography system. The profiles of interface progression are analyzed to underpin the mechanisms of enhanced solvent mass transfer during solvent extraction processes such as “surface renewal” and “sloughing”. The specific objectives are addressed below:

- 1) Investigating the effect of pentane-octacosane interface orientation on interface displacement rate.
- 2) Investigating how the pentane-octacosane interface progresses, continuous or discontinuous, as pentane diffusing octacosane in the bulk condition.
- 3) Studying the kinetic of solvent-assisted bitumen and heavy oil production processes in high permeability reservoirs.
- 4) Evaluating if the enhanced solvent mass transfer during solvent extraction processes can be explained by “surface renewal” or “sloughing” mechanisms.

1.4 Thesis Outline

Chapter 1 presents the research background, problem statement and specific objectives of this dissertation.

Chapter 2 reviews heavy oil and bitumen reserves, thermal recovery methods and emphatically the theory of solvent-assisted bitumen production methods.

Chapter 3 includes methodology, experimental setup, and detailed experimental procedures.

Chapter 4 presents experimental results as well as analysis and discussion of experimental findings.

Chapter 5 exclusively summarizes experimental findings and provides recommendations for future works.

CHAPTER 2 LITERATURE REVIEW

2.1 Heavy Oil and Bitumen Resources

It is estimated that there is a total of 1,350 billion barrels of bitumen resources deposited in Alberta, Canada (Mossop, 1980). There are four major heavy oil basins in Canada as shown in **Figure 2-1**, among which the Athabasca oilfield holds the largest oil sands deposit of 869 billion barrels of bitumen in place (Mossop, 1980). With increasing energy demand and continuous depletion of conventional oil reserves, the petroleum industry is shifting its focus to heavy oil and bitumen resources (Hein, 2017; Nasr and Ayodele, 2006). According to the Alberta Energy Regulator, the total crude bitumen production, including surface mining and *in-situ* production, reached 3 million barrels per day (Mbbbl/d) in 2018, and the projected production rate in 2028 is around 4 Mbbbl/d (Alberta Energy Regulator, 2019).

The properties of Canadian heavy oil reservoirs are listed in **Table 2-1**. In comparison with conventional light oils, the most outstanding characteristic of heavy oil and bitumen is their extremely high viscosities (Speight, 2014). Heavy oils usually have viscosities in the range of 500 to 20,000 cP (PetroWiki, 2020). The viscosity of bitumen and extra-heavy crude oil can be up to hundreds of thousands of centipoises with API gravity of less than 12 °API at reservoir conditions (Lin, 2014; Speight, 2014). Owing to such high viscosity, bitumen cannot flow to a production well in its natural state without reservoir stimulations (Hart, 2014).

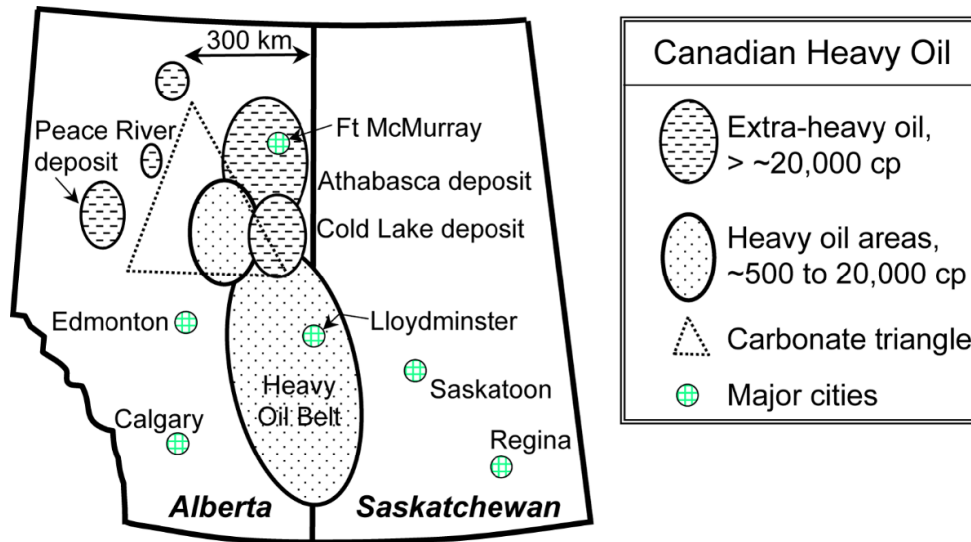


Figure 2-1. Major heavy oil reserves in Canada (PetroWiki, 2020).

Table 2-1. Characteristics of typical Canadian heavy oil reservoirs (Dusseault, 2001; James et al., 2007; Lin, 2014).

Property	Value
Pay zone thickness	5 – 65 m
Maximum depth	800 – 1000 m
Reservoir temperature	4 – 40 °C
Porosity	0.26 – 0.32
Permeability	1.2 – 7.5 Darcy

2.2 The Thermal Recovery Methods

The early-stage exploitation methods include thermal recovery processes such as Steam-Assisted Gravity Drainage (SAGD), Cyclic Steam Stimulation (CSS), and *in-situ* Combustion (ISC) (Boberg, 1988; Shah et al., 2010). The core mechanism of thermal stimulation methods is to heat the crudes to reduce their viscosity so that they flow (White and Moss, 1965). While these methods have been widely used in field applications, they come with a few well-known drawbacks. The capital cost for generating high-quality steam is typically high (Chaar et al., 2015). The energy efficiency is typically low due to steam channeling and heat loss to the formation, especially in thin reservoirs (Wang, 2010). The injected steam condenses in the well and mixes with oil (Ovalles, 2019). This increases operational costs for liquid handling and separation (Zerkalov, 2015) and potential environmental impacts (Wu et al., 2019). Thermal methods may also cause formation damage such as clay swelling, permeability reduction and blockage of production path (Zhang and Chen, 2018). As environmental regulation tightens, ongoing water usage and disposal of contaminated water pose challenges (Swenson et al., 2012).

2.3 The Solvent-Assisted Recovery Methods

Solvents, such as propane, butane, and pentane etc., can be injected alone or co-injected with steam to produce heavy oils and bitumen (Gates and Chakrabarty, 2006; Leyva-Gomez and Babadagli, 2016; Rezaei et al., 2010; Upreti et al., 2007; Wang et al., 2014). The viscosity of heavy oil and bitumen is reduced significantly even for a small solvent mass fraction (Pathak et al., 2011; Pathak et al., 2012). Solvent injection reduces or eliminates steam usage, and in the case of solvent co-

injection can improve production rates (Ardali et al., 2011). The energy intensity of the production processes is also reduced along with GHG emissions (Gates, 2010; Suranto et al., 2015). Solvent diffusion is slow relative to heat transfer at the pore scale (Bayestehparvin et al., 2015). Diverse explanations have been proposed for observed production enhancements. For example, Jyotsna and Gates (Jyotsna and Gates, 2010) suggested that interface instability enhances mixing leading to higher production rates arising from co-injection than those from steam injection alone. Das and Butler (Das and Butler, 1994a) injected propane vapor into bitumen and attributed the enhancement to deasphalting. Diluted and deasphalted bitumen has a low viscosity and can be produced more quickly.

2.3.1 Solvent Chamber Evolution

There are three stages during solvent extraction processes including the solvent chamber rising, spreading, and falling phases as shown in **Figure 2-2** (Lin, 2014). In this figure, the letters “I” and “P” represent injection and production wells, respectively. Initially, solvents are injected through the injection well. The solvent chamber keeps rising until reaching the top of the formation, usually an impermeable rock layer. Then, it is followed by the solvent spreading phase. Solvents continue to spread laterally until reaching boundaries of the formation. Finally, the solvent-bitumen interface starts to fall with decreasing bitumen production rates. In general, the spreading phase takes a much longer time than the other two phases as the width of the formation is greatly larger than formation thickness. As a result, the majority of bitumen production occurs during this phase.

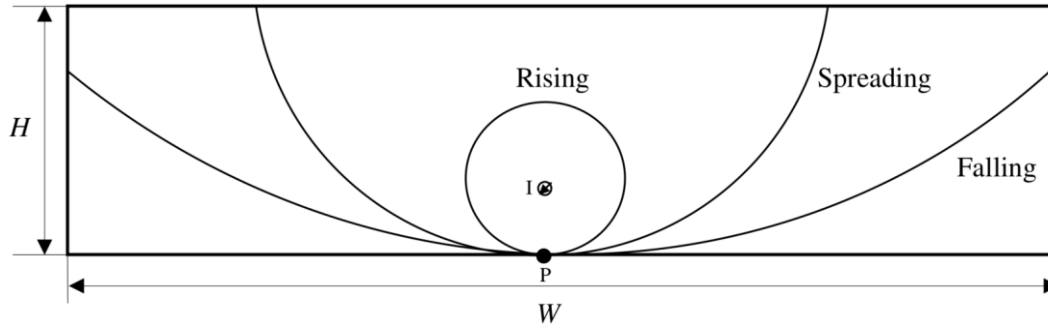


Figure 2-2. Schematic of the solvent rising, spreading, and falling phases during solvent extraction processes (Lin, 2014).

2.4 Mathematical Model of the Solvent Recovery Method

Butler and Mokrys (Butler et al., 1985; Das and Butler, 1998; Mokrys and Butler, 1993) developed a two-dimensional solvent analog model of the SAGD process to theoretically describe the solvent lateral spreading phase of a solvent vapor extraction (VAPEX) process. The model employs gravity drainage in a horizontal well pair to recover solvent-diffused bitumen. In their model, they assumed that solvent diffusion is similar to heat transfer. They also experimentally verified the analog model by using toluene as the extracting solvent to recover bitumen in a Hele-Shaw cell with a wide range of permeability at room temperature and atmospheric pressure (Mokrys and Butler, 1993). **Figure 2-3** shows a schematic representation of solvent extracting bitumen processes inside a Hele-Shaw cell. The cell consists of two glass plates uniformly separated by inserting metal foil at the edges. Three sides of the cell are sealed with a silicone compound, and then it is filled with bitumen (Butler et al., 1985). The solvent is injected from the upper-left corner of the cell in contact with and diffuses into bitumen. The diluted bitumen with reduced viscosity drains down along the solvent-bitumen interface to the production outlet at the lower-left corner.

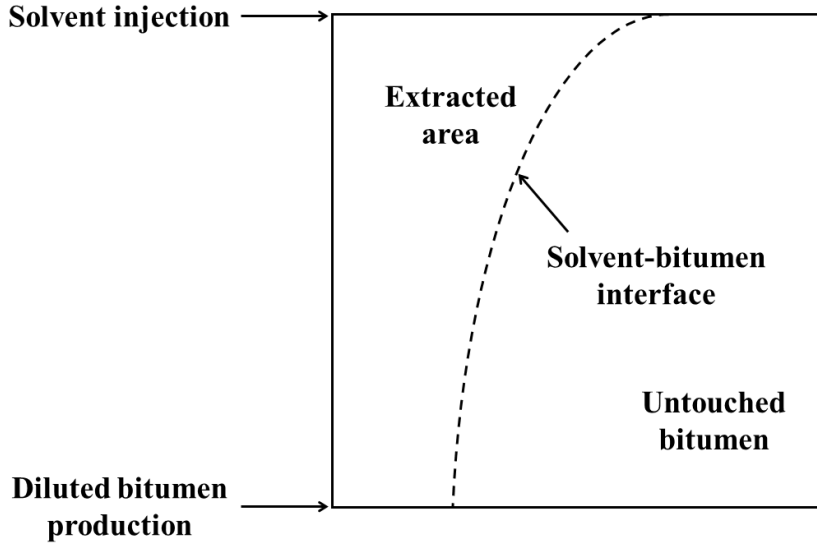


Figure 2-3. Schematic of a Hele-Shaw cell.

Figure 2-4 shows a schematic of a diffusion layer of the Butler-Mokrys solvent analog model. A layer of diluted bitumen with a thickness of “ ξ ” continuously drains down with constant velocity “ v ” as solvent diffusing. The solvent-bitumen interface advance at constant speed of “ U ”. The mathematical model for estimating the bitumen production rate is presented as:

$$Q = \sqrt{2kg\phi\Delta S_o N_s h} \quad [2-1]$$

$$N_s = \int_{c_m}^{c_i} \frac{\Delta\rho D_s (1 - c_s)}{\mu c_s} dc_s \quad [2-2]$$

where, Q is the bitumen drainage rate (m^2/s); k is the Hele-Shaw cell permeability (μm^2); g is the gravitational acceleration (m/s^2); ϕ is the Hele-Shaw cell porosity; ΔS_o is the change in oil saturation; h is the height of the Hele-Shaw cell (m); N_s is a dimensionless number defined by

equation [2-2]; c_m is the minimum concentration of solvent in solvent-bitumen mixture required to mobilize; c_i is the solubility of the solvent vapor in bitumen; c_s is the volume fraction of solvent in diluted bitumen; $\Delta\rho$ is the density difference between the diluted bitumen and pure solvent (kg/m^3); μ is the viscosity of diluted bitumen (cP); D is the intrinsic diffusivity of solvent in bitumen (m^2/s). Details of the Butler-Mokrys Model derivation are available elsewhere (Das and Butler, 1998). Base on **Equation [2-1]**, Das and Butler (Das and Butler, 1998) defined the Vapex parameter as:

$$a = \sqrt{2kg\phi\Delta S_o N_s} \quad [2-3]$$

where a is the Vapex parameter ($\text{cm}^{1.5}/\text{hr}$). They also assumed that for the same bitumen-solvent liquid system, at the same experimental conditions, the values of “ N_s ” of porous media with different permeabilities are equal. The Vapex parameters of two different porous media have a relationship as:

$$\frac{a_1}{a_2} = \sqrt{\frac{k_1\phi_1\Delta S_{o_1}}{k_2\phi_2\Delta S_{o_2}}} \quad [2-4]$$

where subscripts “1” and “2” represent the porous media 1 and 2, respectively. As a result, the production rates of these two porous media have a relationship as:

$$\frac{Q_1}{Q_2} = \frac{a_1}{a_2} \sqrt{\frac{h_1}{h_2}} \quad [2-5]$$

Assumptions in the Butler-Mokrys model include: (1) the interface progresses parallelly; (2) the interface advances at a constant rate; (3) solvent diffusion follows Fick’s law; (4) diluted bitumen

flows continuously as a film; (5) fluid flow follows Darcy's law; (6) there are no radial velocity, concentration, density, or viscosity gradients. They supported their model experimentally using toluene as a solvent to produce bitumen from a Hele-Shaw cell with a wide range of permeability at room temperature and atmospheric pressure (Mokrys and Butler, 1993).

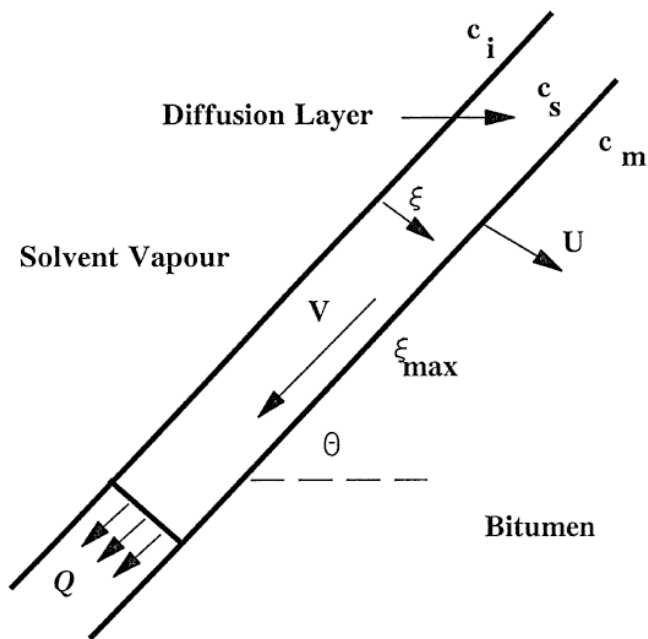


Figure 2-4. Schematic of the diffusion layer of the Butler-Mokrys model (Das and Butler, 1998).

2.5 Experimental Study of the VAPEX Model

Das and Butler (Das and Butler, 1994a; Das and Butler, 1995; Das and Butler, 1994b) performed a series of experiments to test whether the Butler-Mokry's model can predict bitumen production rates in presence of porous media. They used butane to extract Lloydminster bitumen in a Hele-Shaw cell (experiment 1) and a sand-packed cell (experiment 2). In experiment 1, the porosity " ϕ " and the change of oil saturation " ΔS_o " are equal to one. The bitumen production rate is calculated by determining the area between two consecutive drainage curves during a time interval (Das and Butler, 1994a). The Vapex parameter " a_1 " is then calculated by **Equation [2-3]**. Based on the assumption discussed above, the predicted Vapex parameter " a_2 " for experiment 2 is determined by **Equation [2-4]**. The predicted production rate " Q_2 " is then calculated based on **Equation [2-5]**. The actual production rate of experiment 2 is obtained by collecting fluid at the outlet of sandpack cell. Based on the experimental results shown in **Table 2-2**, Das and Butler (Das and Butler, 1994b) found that actual bitumen production rates from sand-packed cells (experiment 2) are 3 to 5 times greater than those predicted by the Butler-Mokry's model. They attributed the enhancement to "surface renewal" (Das and Butler, 1998) based on periodic striations of asphaltene deposition on cell walls shown in **Figure 2-5**. As the solvent diffuses into bitumen to lower its viscosity, a layer of diluted bitumen becomes mobile and drains down along the diluted bitumen-bitumen interface. A new solvent-bitumen interface is then created with a sharp solvent concentration profile across the interface resulting in a higher solvent mass transfer rate — also referred to as "concentration shock". Periodic interface renewal augments the constant solvent-bitumen interface advancement rate built into the Butler-Mokry's model.

Table 2-2. Comparison of predicted and actual bitumen production rates in sand-packed cells
(Das and Butler, 1994b).

Cell/solvent Temperature (°C)	Cell & Permeability (Darcy)	Vapex Parameter: Scaled up from Hele-Shaw Cell Results (cm ^{1.5} /hr)	Vapex Parameter (cm ^{1.5} /hr) Experiment	Stabilized Rates Predicted (gm/hr)	Flow Rates Experiment (gm/hr)
22.0 / 21.3	Hele Shaw 5400	4.35	4.35	–	–
22.0 / 21.1	Visual 830	0.94	2.67	13.70	39.70
22.0 / 21.5	Visual 217	0.48	1.6	7.13	25.10
22.0 / 21.0	Visual 43.5	0.21	1.01	3.12	15.60

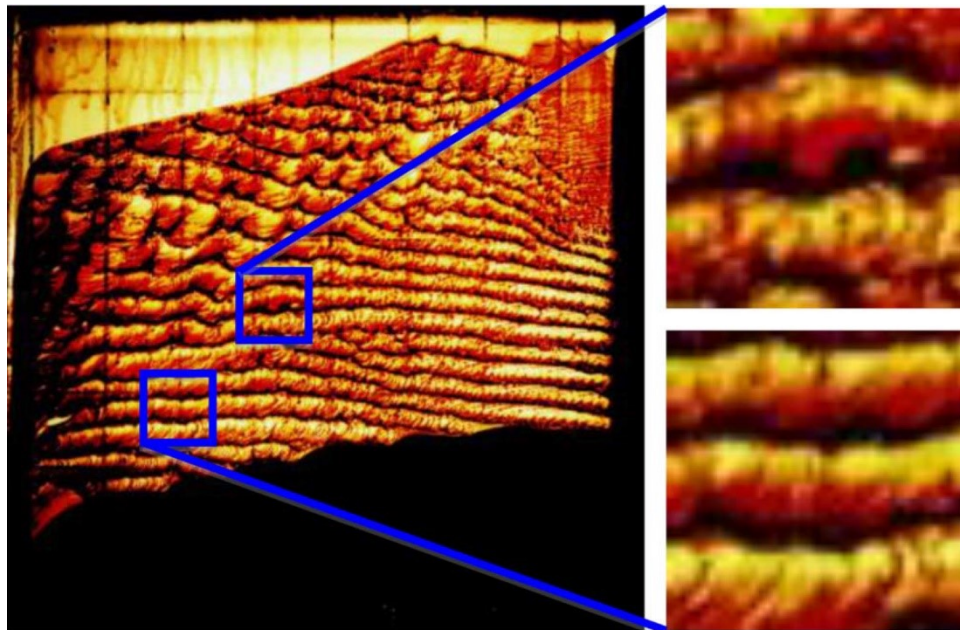


Figure 2-5. Periodic asphaltene deposition observed on a Hele-Shaw cell from a VAPEX experiment (Das and Butler, 1998).

2.6 Hypothesis of the “Sloughing” Phenomenon

Stewart and Shaw (Stewart and Shaw, 2018) analyzed the discrepancies between penetration values predicted by the Butler-Mokry model and experimentally measured ones. They proposed that during a solvent-assisted bitumen extraction, interfacial tension (IFT) plays a crucial role (Argüelles-Vivas et al., 2012; Naderi et al., 2015; Stewart and Shaw, 2018; Yang and Gu, 2005). The bitumen-water interfacial tension is reduced by up to two orders of magnitude when adding 10-30 wt% solvent to bitumen (He et al., 2014). Solvent diffusion into bitumen causes an imbalance of forces. As the gravitational force overcomes the interfacial force, bitumen-rich drops disengage from the bitumen body and flow away. This process is referred to as “sloughing” shown in **Figure 2-6**.

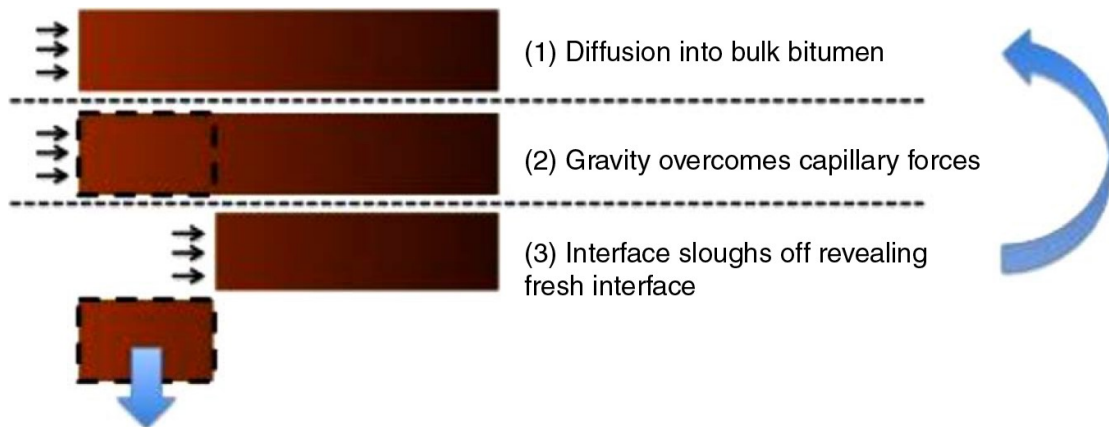


Figure 2-6. Mechanisms of sloughing events (Stewart and Shaw, 2018).

Figure 2-7 shows a schematic of energy exchange inside a pore during bitumen drop mobilization. Initially, bitumen is trapped inside a water-wetting pore. The energy exchange during a “sloughing” event renews solvent-water and solvent-bitumen interfaces and provides kinetic energy to the bitumen-rich drops (Stewart and Shaw, 2018). If assuming the IFT between two liquids does not vary as liquid properties modify ($\sigma_{WS} = \sigma'_{WS}$; $\sigma_{BS} = \sigma'_{BS} = \sigma''_{BS}$) and the surface area of the bitumen liquid changes insignificantly ($A_2 = A_8$), the potential energy change needs to overcome the requirement of interfacial-energy-generation is expressed as:

$$\Delta E = (\sigma_{WS} + \sigma_{BS} - \sigma_{WB})A + gH(\rho_B - \rho_S)V_B \quad [2-6]$$

where ΔE is the drop mobilization energy; A is the surface area of the bitumen drop; σ are the interfacial tensions between water and solvent, bitumen and solvent, and water and bitumen denoted with subscripts of “*WS*”, “*BS*” and “*WB*”, respectively; H is the change of the center of gravity; ρ are the densities of bitumen and solvent denoted with subscripts of “*B*” and “*S*”; V_B is the volume of bitumen drops. The drop mobilization energy ΔE must be positive for a liquid bitumen drop to flow away from the pore. The discontinuous flow results in a solvent “concentration shock” across the solvent-bitumen interface. The mass transfer rate is enhanced after each sloughing event. **Figure 2-8** shows conceptually how the solvent-bitumen interface displacement is enhanced by “sloughing”. The interface displacement depth and rate exceed continuous displacement after a few cycles of “sloughing” events (Stewart and Shaw, 2018).

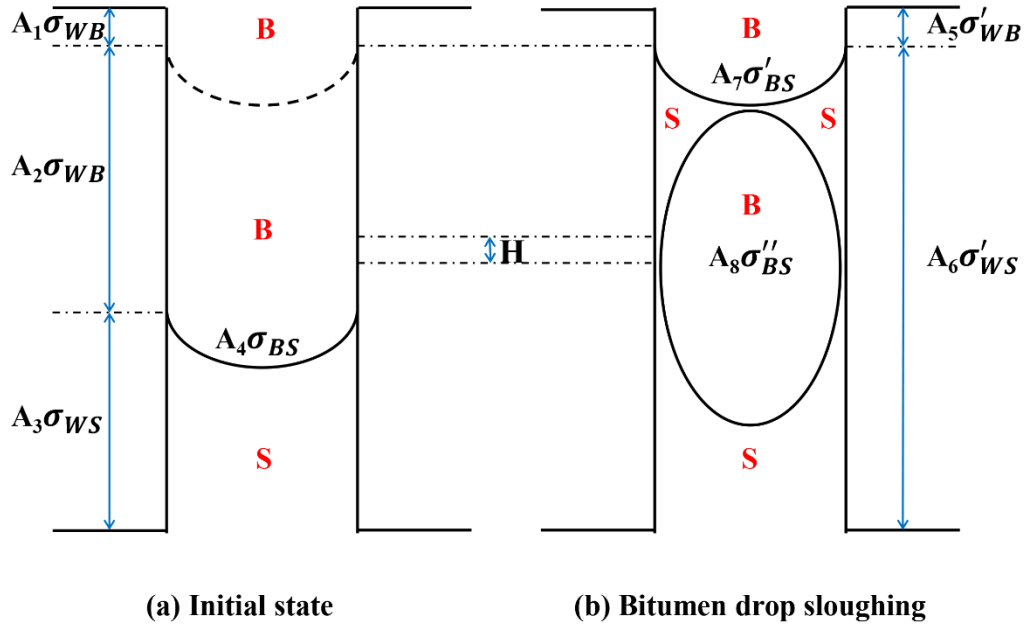


Figure 2-7. Energy exchange during drop mobilization. The letter “S” and “B” represent solvent and bitumen phases, respectively.

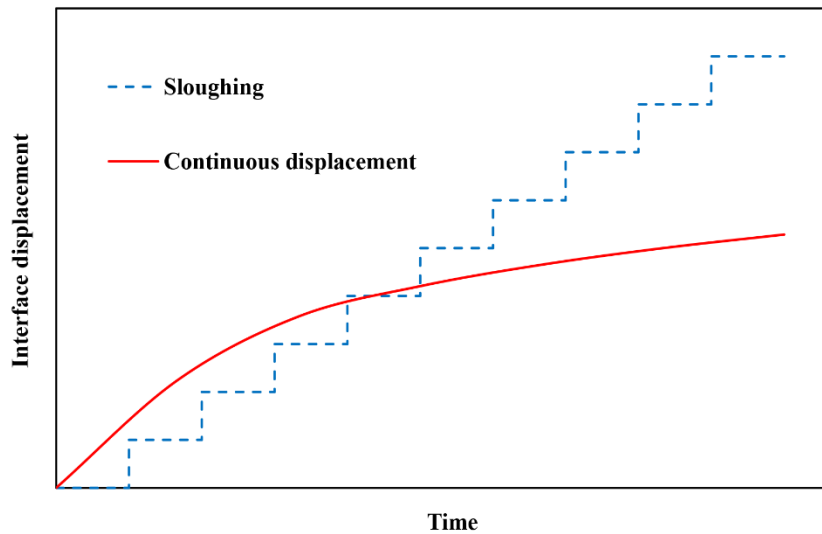


Figure 2-8. Theoretical comparison of the interface displacement rates between continuous interface advancements and the “sloughing” mechanism.

2.7 Solvent Diffusivity in Bitumen

To develop robust models for such complex solvent-assisted bitumen production processes, the physics of “surface renewal” or “sloughing” events must be quantified and discriminated from the contribution of diffusion to production rates. Liquid phase mutual diffusion and enhanced mass transfer arising from shear adjacent to liquid–immobile liquid or solid interfaces provide clear starting points for understanding and parsing these interfacial mass transfer processes. These phenomena are well-defined and well-understood in the literature, including theoretical and experimental examples related to heavy oils and bitumen. For example, liquid-phase mutual diffusion coefficients for solvents in heavy oils and bitumen are bounded by theory and for specific cases best obtained from direct measurement of local composition profiles within a liquid phase (Tharanivasan et al., 2004; Zhang et al., 2007; Zhang and Shaw, 2007). Reported mutual diffusion coefficient values, at ambient conditions, are low ($\sim 10^{-10}$ m²/s) and the corresponding measured solvent penetration rates, over durations exceeding days, where the solvent is above and the bitumen or heavy oil is below the interface, are also low (~ 0.01 μm/s). With forced convection, leading to high shear at a solvent–heavy oil or bitumen interface, penetration rates up to three orders of magnitude greater than those obtained for diffusive penetration alone can be realized (~ 10 μm/s) (Sadighian et al., 2011). While such enhanced penetration rates are consistent with conventional liquid-liquid and liquid-solid mass transfer predictive models and theory, the required shear rates cannot be realized without mechanical agitation and cannot be produced in a micro porous medium. Consequently, solvent enhanced production rates cannot be attributed to diffusion alone. Dunn and Nenniger (Dunn et al., 1989) studied the soluble-gas injection bitumen recovery process both theoretically and experimentally based on the principles of thermal gravity drainage. The predicted drainage rate underestimated the experimental production rate for

experiments conducted at 20 °C in a glass bead-packed cell where carbon dioxide and ethane gases were injected into Athabasca bitumen. They proposed a concept of “effective diffusivity”, which is two to three orders of magnitude greater than the reported liquid-phase mutual diffusivity values, to match their experimental production data. However, in a two-fluid system, the mutual diffusion coefficient should fall in the range of the tracer diffusion coefficient and the self-diffusion coefficient (Stewart and Shaw, 2018). The effective diffusivity discussed above should also be in this range to be physically correct. A similar conclusion can also be obtained if calculating the “effective diffusivity” based on Das and Butler’s experimental data (Das and Butler, 1994b). As shown in **Figure 2-9**, the solvent effective diffusivity in bitumen is around three orders of magnitude higher than the solvent-bitumen mutual diffusion coefficient ($\sim 10^{-10} \text{ m}^2/\text{s}$). The detailed calculation can be found in **Appendix A**.

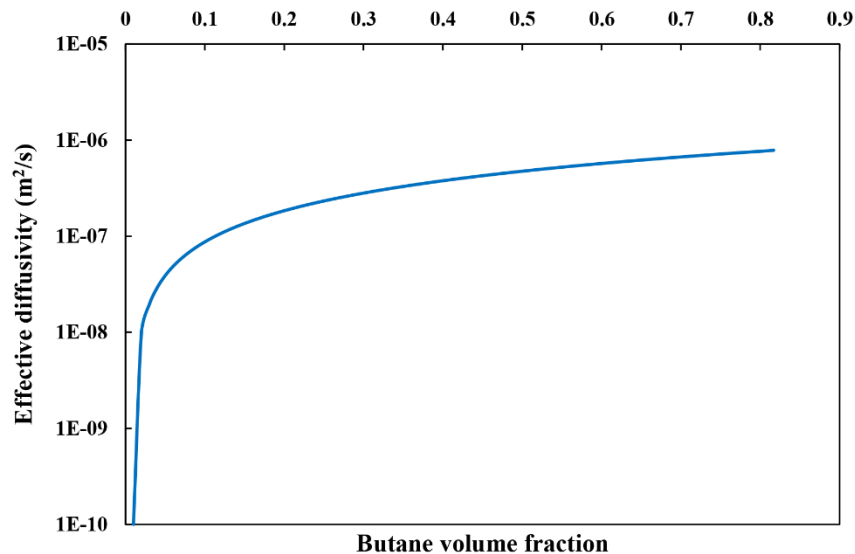


Figure 2-9. Butane effective diffusivity calculated based on Das and Butler’s experimental results (Das and Butler, 1994b).

CHAPTER 3 EXPERIMENT SECTION

3.1 Methodology

X-ray videography is employed to study the penetration of n-pentane into octacosane and to observe “surface renewal” and “sloughing” directly. Octacosane, a wax, acts as a well-defined surrogate for immobile bitumen. Carefully calibrated high-resolution X-ray videos and still images are analyzed to obtain intensity profiles and track the locations of interfaces versus time. Pentane-octacosane interface orientation is manipulated to investigate the effect of interface orientation on interface progression rates.

3.2 Experimental Setup

Solvent-wax systems (n-pentane + octacosane) were prepared in 95 mm long by 25 mm diameter (VWR, 470177-990) glass vials with the orientations illustrated in **Figure 3-1**. The chemicals used, their sources and purities are listed in **Table 3-1**. The movement of the interface is monitored using high-resolution X-ray videography. The main components of the X-ray equipment include glass vials, an X-ray gun, a camera, a cooling system, and a computer imaging system as shown in **Figure 3-2**. Video stills were analyzed using ImageJ[™], with a pixel size of 170 μm and a time resolution of 0.033 s. All measurements were conducted at ~ 22 °C and atmospheric pressure. Details of the X-ray set-up and its operation are available elsewhere (Dini et al., 2016).

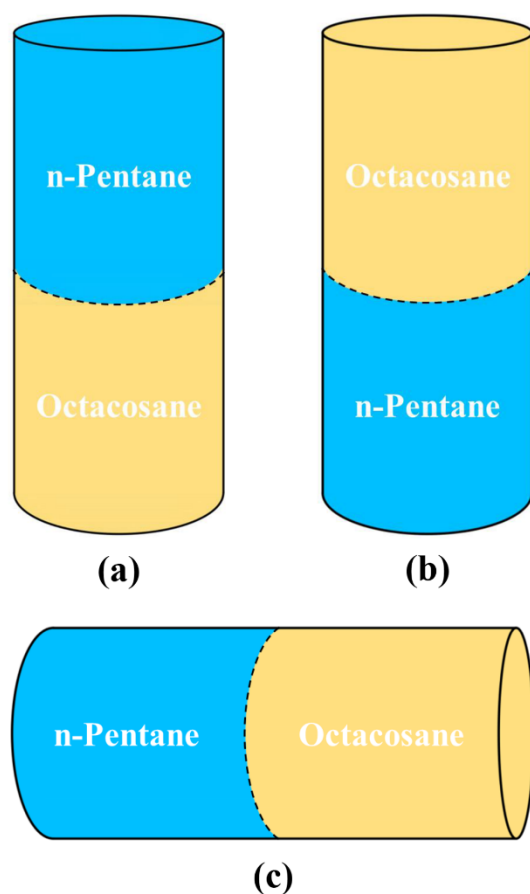


Figure 3-1. Schematic representations of the interface orientations and geometries: (a) horizontal interface with octacosane below; (b) horizontal interface with pentane below; (c) vertical interface.

Table 3-1. List of chemicals used in experiments

Chemicals	Properties	Purity	Manufacturer
n-Pentane (C ₅ H ₁₂)	Liquid density: 0.6238 g/ml (Burgess, 2012)	99.7%	Fisher Scientific
Octacosane (C ₂₈ H ₅₈)	Solid density: 0.8067 g/ml Melting point: 59-65 °C (Haynes, 2016)	99.0%	Sigma-Aldrich

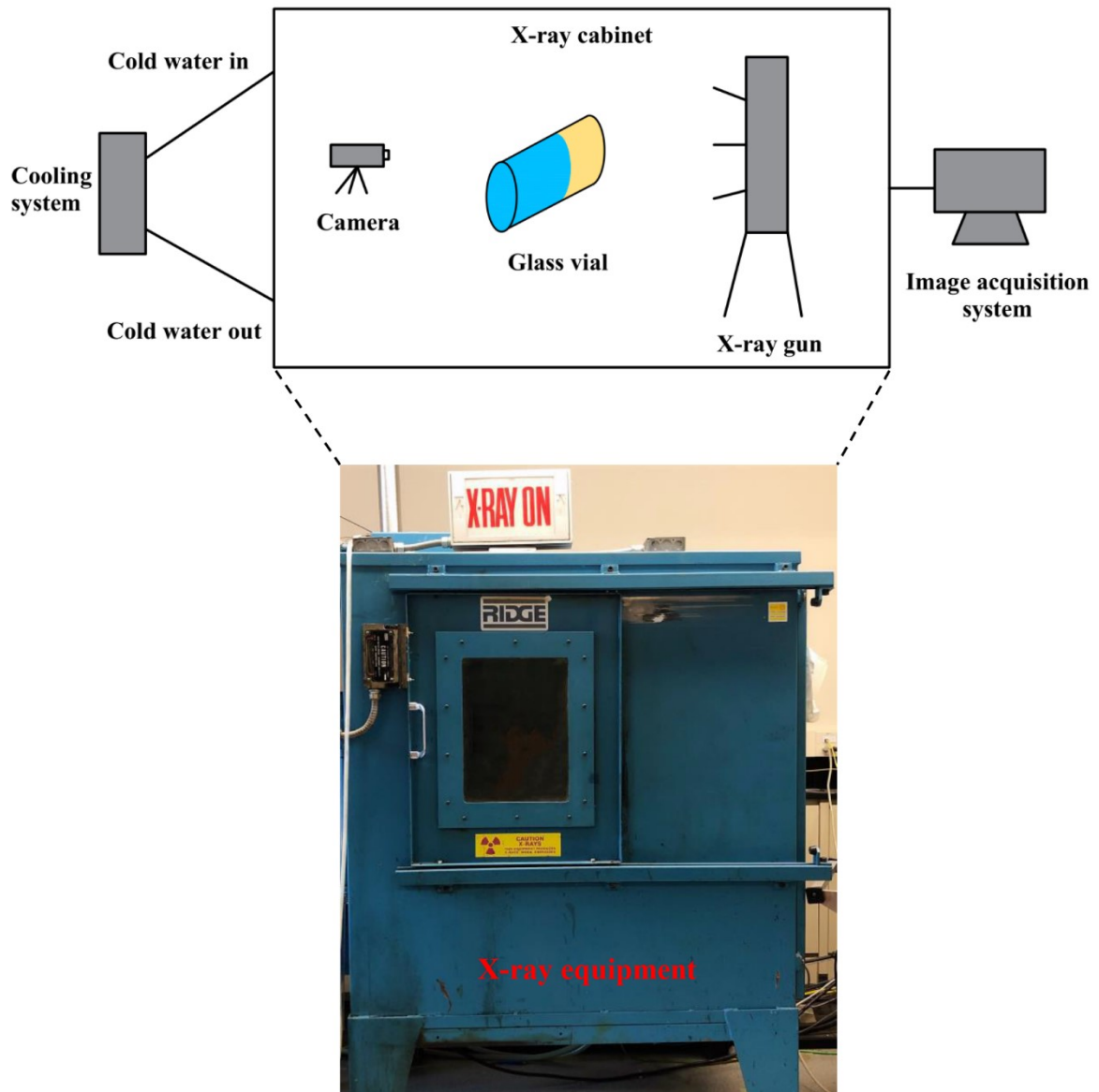


Figure 3-2. The Schematic of the X-ray system.

3.3 Experimental Procedure

3.3.1 Sample Preparation

There are four major steps required to create the solvent-wax systems including: melting and transferring the octacosane, solidifying it, carving and flattening the surface, and adding pentane, as shown in **Figure 3-3**. The detailed procedure is: (1) transfer 20 g of octacosane into a 100 ml beaker; place the beaker, a glass funnel, and a glass stirrer in the oven; set the oven temperature to 100 °C and wait for about 30 minutes for the wax to reach the target temperature; (2) half fill the glass vial with liquid octacosane as shown in **Figure 3-3(a)**; quickly place the glass vial into the ice-bath; put the remaining liquid octacosane into the oven to keep it at 100 °C; (3) use a glass stirrer to gently stir the wax as it solidifies to create a regular cylindrical hole in the surface as shown in **Figure 3-3(b)**; (4) fill the hole as shown in **Figure 3-3(c)** with more liquid octacosane and use the same cooling technique to create a smaller hole; repeat until the hole is filled; (5) use a steel spatula to shape and flatten the octacosane surface and remove excess octacosane from the vial walls; (6) verify the flatness of the surface in the X-ray unit; (7) place the glass vial vertically in a beaker; fill the vial with n-pentane; seal the vial with a plug ensuring there is no air bubbles trapped inside the vial as shown in **Figure 3-3(d)**; (8) place the glass vial vertically or horizontally in the X-ray unit as shown in **Figure 3-1(a)**, **Figure 3-1(b)** or **Figure 3-1(c)**; turn the X-ray system on to record the interface movement with time. The flow chart of experimental procedures is presented in **Appendix B**.

3.3.2 X-ray System Operation

The X-ray system must be stabilized prior to use. First, the cooling system for the X-ray source and the detector is turned on. Then, the X-ray source is conditioned at 120 kV for 20 minutes.

After that, the operating conditions are set at 45 kV, 3.35 mA, and 0.5 focus and measurements can be performed. Interface displacement data are presented at either 0.5 s or 10 s intervals as indicated in Figure captions.

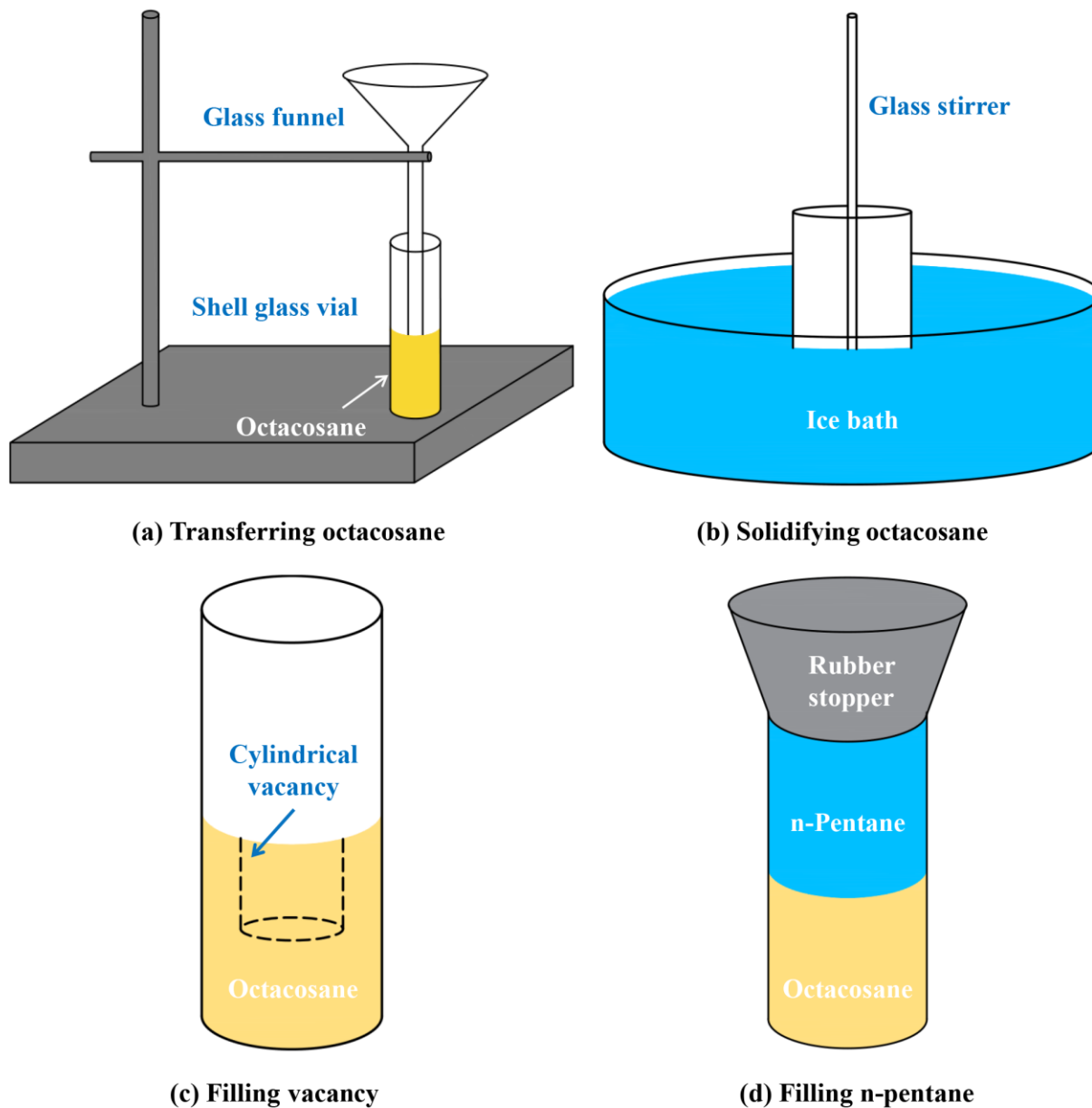


Figure 3-3. Procedures of creating the pentane-octacosane interfaces.

CHAPTER 4 RESULTS AND DISCUSSION

4.1 Overview

Four sets of experiments including one control experiment were performed. The control experiment illustrates the flatness of the octacosane surface, the resolution of the interface within the composition depth profiles, and the consistency of the intensity measurements within each phase. The other three experiments concern interface displacement for the n-pentane + octacosane system orientations shown in **Figure 3-1**. Octacosane has a lamellar crystal structure. The cohesion within it is weak (Dorset, 2000; Žbik et al., 2006). The solubility of octacosane in n-pentane at the experimental conditions is ~ 0.014 (mole fraction) (Madsen and Boistelle, 1976) or ~ 0.073 (mass fraction). The density of this saturated solution is $\sim 639 \text{ kg/m}^3$. These properties and property differences relative to n-pentane establish driving forces for diffusion and convection at the pentane-octacosane interface.

4.2 Air + Octacosane System

Figure 4-1 shows an annotated X-ray video still of the air-octacosane system adjacent to the air-octacosane interface. The light gray phase on the left is filled with air, and octacosane is placed on the right with a darker gray color. The surface of solid state octacosane is flattened by using a spatula as described previously. As shown in the figure, the octacosane surface is visually smooth and level across the cross-section of the vial and the octacosane phase is visually uniform. After

adding pentane into glass vial, pentane can contact octacosane evenly and diffuse into it. A sharp interface makes the observation of pentane-octacosane interface movement easier.

Figure 4-2 shows the intensity profile obtained from the area of interest with a length of 15 mm and a height of 2 mm dictated in **Figure 4-1**. The intensities of 12 pixels (~ 2 mm) are averaged at each elevation. The horizontal axis is a length scale where the origin is the right-hand side of the selected area, and the vertical axis is a dimensionless gray scale. The gray scale value is a measure of intensity or optical density. While there is no direct mathematical relationship between the optical density and mass density, the higher mass density usually corresponds with lower intensity or gray value, and vice versa.

The average intensity of air, on the left-hand side of **Figure 4-2**, is around 37000, and the average intensity of the octacosane on the right-hand side is around 22500. The gray scale values trend slightly within each uniform phase because the X-rays emanate from a point source. The detected intensities are a function of distance and have not been normalized to account for this effect. The local fluctuations in intensity within a uniform phase provide a measure of intensity uncertainty. This uncertainty is small relative to the differences in the intensities of the phases and does not impact interface detection. Interface elevation is defined as the elevation with an intensity midway between the intensities of the two phases. Interfaces have an absolute elevation uncertainty not exceeding one half of a pixel (i.e., less than $85 \mu\text{m}$) for individual measurements.

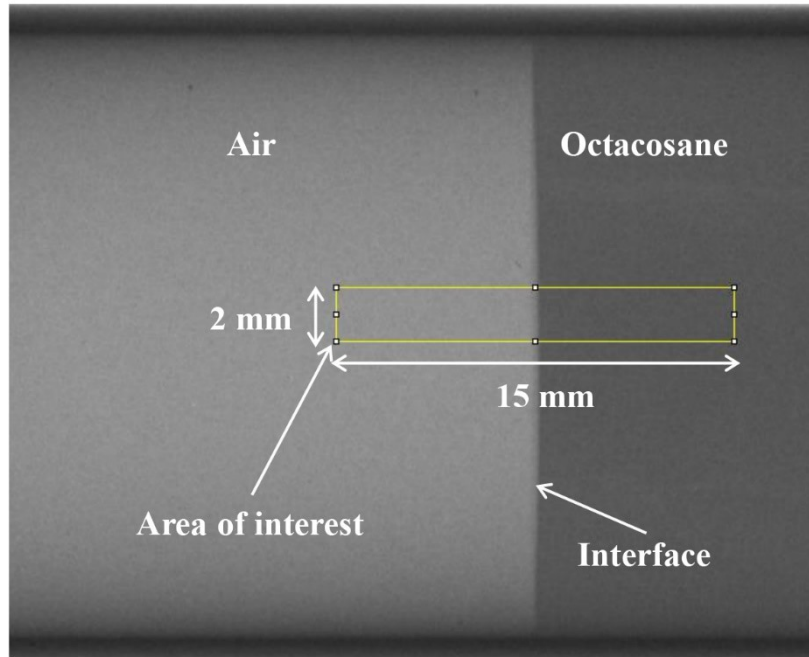


Figure 4-1. X-ray still image showing a cross-section of a glass vial adjacent to an air-octacosane interface. The area of interest is analyzed to obtain the elevation-averaged intensity profile shown in **Figure 4-2**.

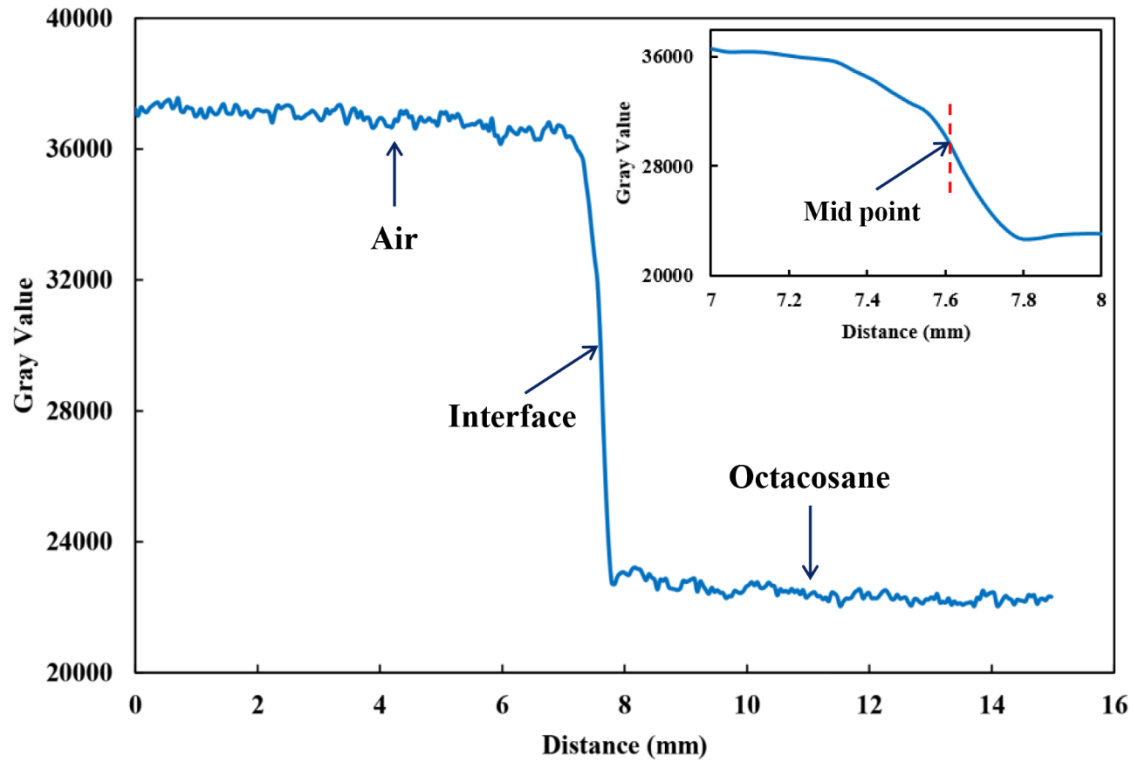


Figure 4-2. Elevation-averaged intensity profile for the area of interest shown in **Figure 4-1**. The midpoint of the interface is highlighted in the inset.

4.3 Horizontal Interface with Octacosane Below

The images obtained from the X-ray videography are further processed by ImageJtm for easier observation of the two phases. For this case, shown in **Figure 4-3**, the octacosane phase with a darker blue color sits below the n-pentane phase. Interface movement is driven by diffusion alone because the octacosane-enriched liquid is denser than pentane. Further, the penetration rate is expected to decrease over time as the liquid boundary layer thickens. The pentane-octacosane interface moves downward slowly as illustrated by **Figure 4-3(a)** and **Figure 4-3(b)**.

Figure 4-4 shows the intensity profile of the area of interest dictated in **Figure 4-3** in 1 hour. The horizontal axis represents the height of this area (15 mm) pointing downward. The gray value at each height is determined as the average cross-sectional intensity. The pentane phase with lower mass density is located on the upper left with higher gray value, and the octacosane phase is on the lower-right. During pentane diffusing octacosane, there is an interface transition zone where the concentration of pentane decreases from 1 to 0. The intensities of the pentane phase ($I_{Pentane}$) and octacosane phase ($I_{Octacosane}$) are calculated by averaging the gray value from the position of 0 to 6 mm and 9 to 15 mm, respectively. The average of pentane-octacosane phase intensities $I_{Interface}$ is given as **Equation [4-1]**. The location of the interface is determined at the position where the gray value is equal to $I_{Interface} = 23500$.

$$I_{Interface} = \frac{I_{Pentane} + I_{Octacosane}}{2} \quad [4-1]$$

The displacement of the interface versus time, shown in **Figure 4-5**, also illustrates the uncertainty

of interface elevation measurement. Over the first 1000 seconds, the interface moves downward from the position of 7.48 mm to 7.54 mm continuously at $\sim 0.06 \mu\text{m/s}$. At the end of one hour, the rate has fallen to $\sim 0.03 \mu\text{m/s}$ —a value trending toward longer-time average values observed for bitumen-solvent interfaces ($\sim 0.01 \mu\text{m/s}$). Along with the solvent diffusion, the pentane-octacosane mixture accumulates near the solvent-wax interface due to its higher density than pure solvent, so the solvent penetration rate is gradually decreasing.

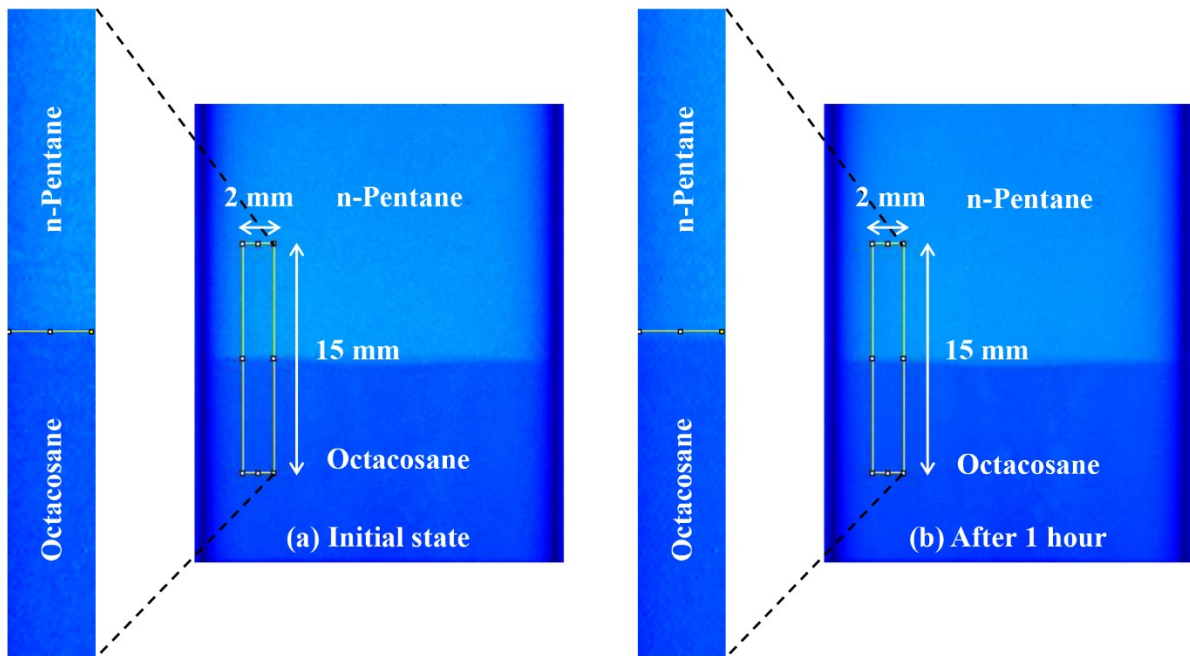


Figure 4-3. Images of the pentane-octacosane system with a horizontal interface (octacosane below): (a) at the initial state and (b) 1 hour later.

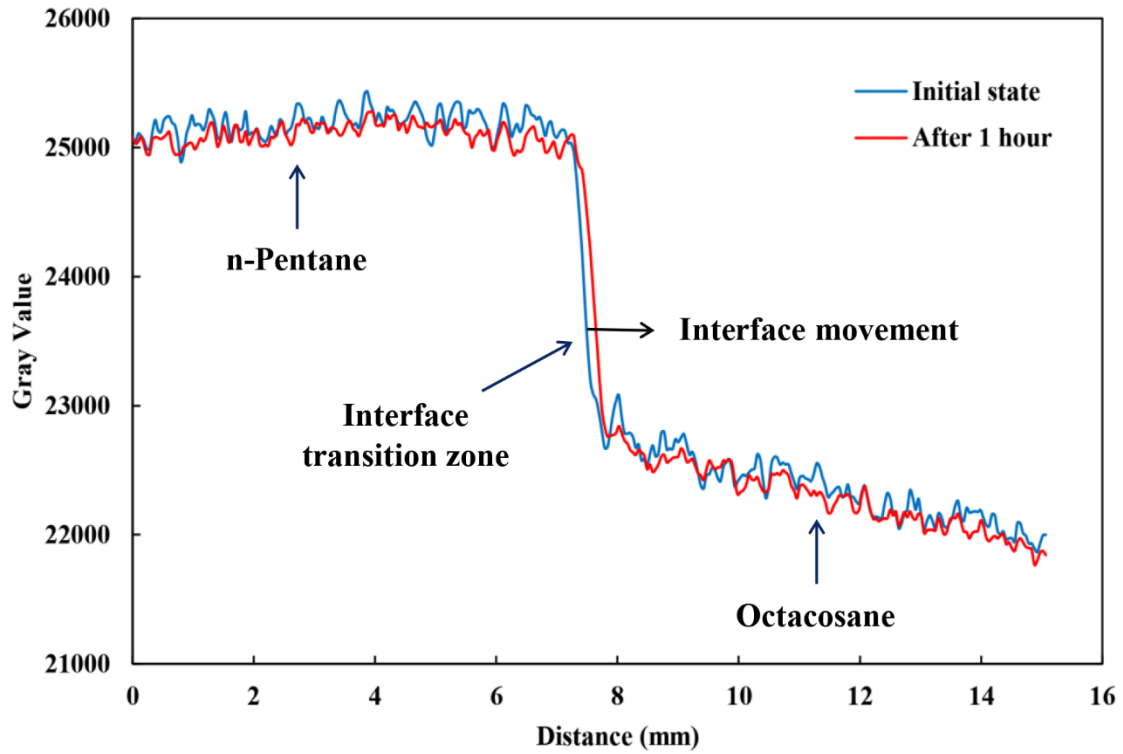


Figure 4-4. Intensity profiles of the areas of interest in the pentane-octacosane system in **Figure 4-3** with a horizontal interface (octacosane below) at the initial state and 1 hour later.

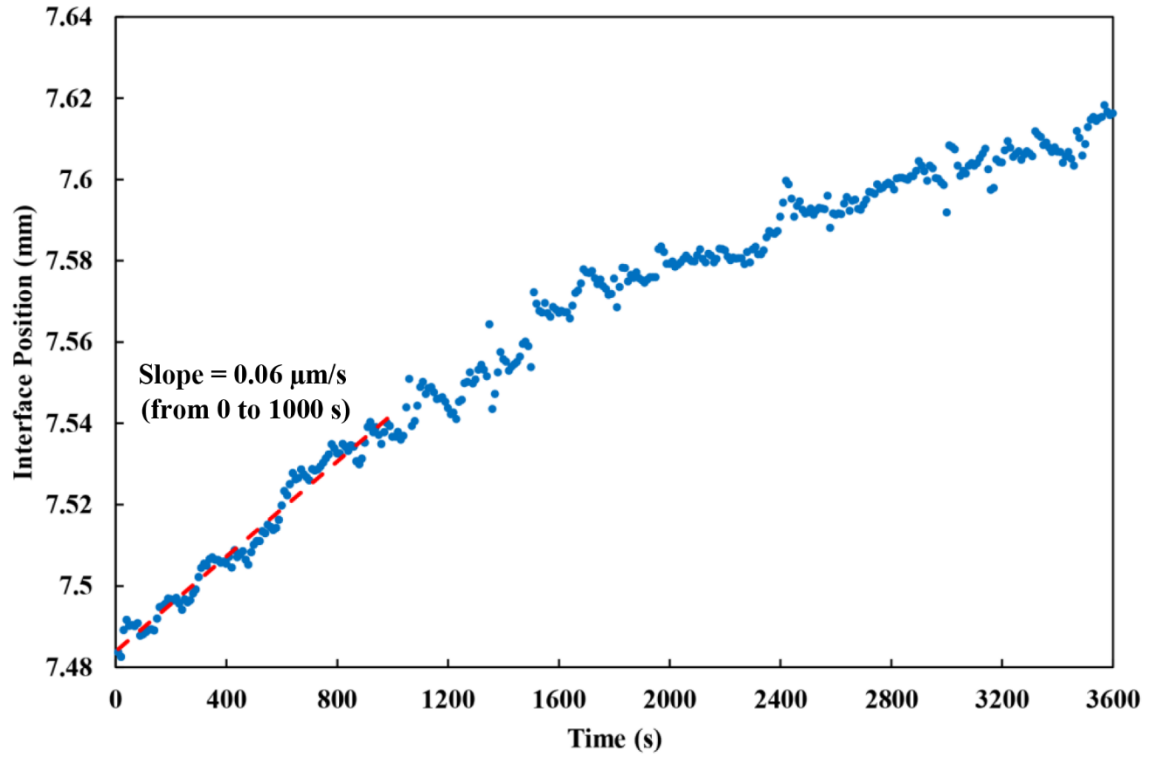


Figure 4-5. Interface displacement for the pentane-octacosane system with a horizontal interface (octacosane below).

4.4 Horizontal Interface with Pentane Below

For this case, two effects are expected. Octacosane dissolving into the pentane raises the local density of the liquid causing it to move downward (away from) the interface. This maintains a high concentration gradient adjacent to the interface that augments the continuous and purely quiescent diffusive displacement described above. The higher-density liquid can also detach from the interface, causing displacement events.

Figure 4-6 illustrates the upward displacement of the horizontal pentane-octacosane interface with n-pentane below. The interface displacement over one hour is visually apparent and readily quantified from the differences in the composition profiles shown in **Figure 4-7**. **Figure 4-8** highlights the upward displacement of the interface for the first 1000 seconds. There are two key features of the displacement process. Displacement is punctuated by episodic jump events every ~ 150 seconds, and the displacement rate in between these events is significantly larger than that for solely diffuse displacement. A time slice from the displacement process, from 520 s to 620 s and highlighted in red in **Figure 4-8**, is presented in **Figure 4-9**. During a 10 s jump event, the interface is displaced by $30 \mu\text{m}$ ($3 \mu\text{m/s}$). Before and after the jump event, the displacement rate is $0.2 \mu\text{m/s}$. Over one cycle, the two effects contribute equally to the displacement of the interface, and over all the displacement rate ($\sim 0.4 \mu\text{m/s}$) is 7 times the initial rate and 40 times the long-term displacement rate for diffusion alone.

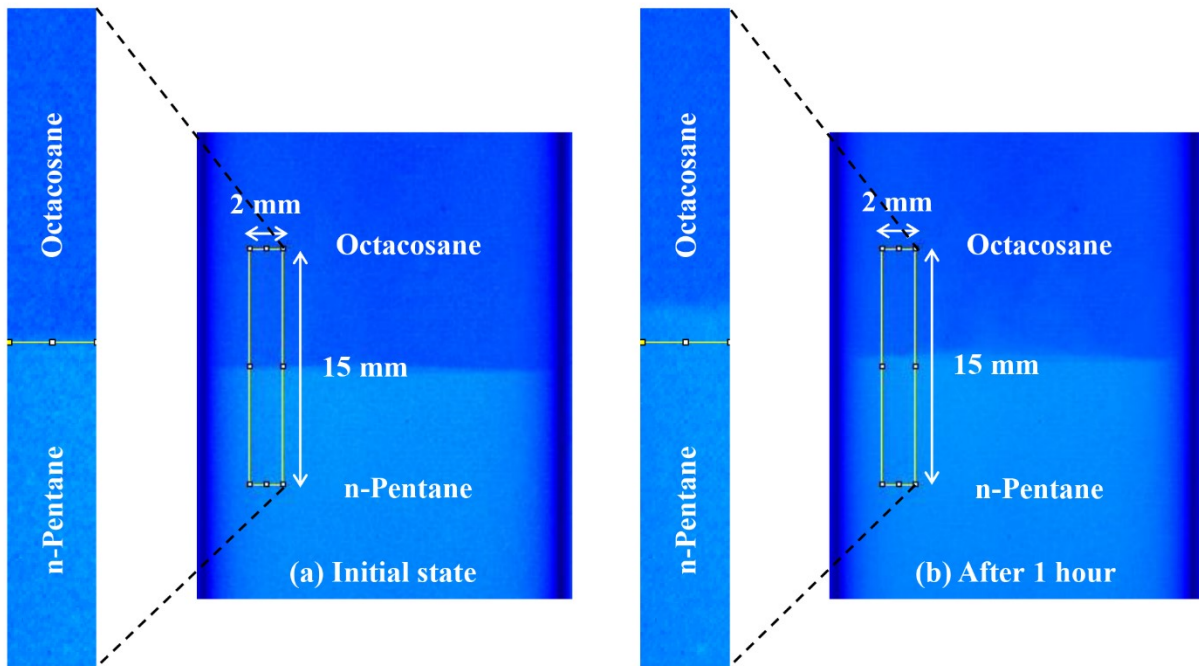


Figure 4-6. Images of the pentane-octacosane system with a horizontal interface (pentane below): (a) at the initial state and (b) 1 hour later.

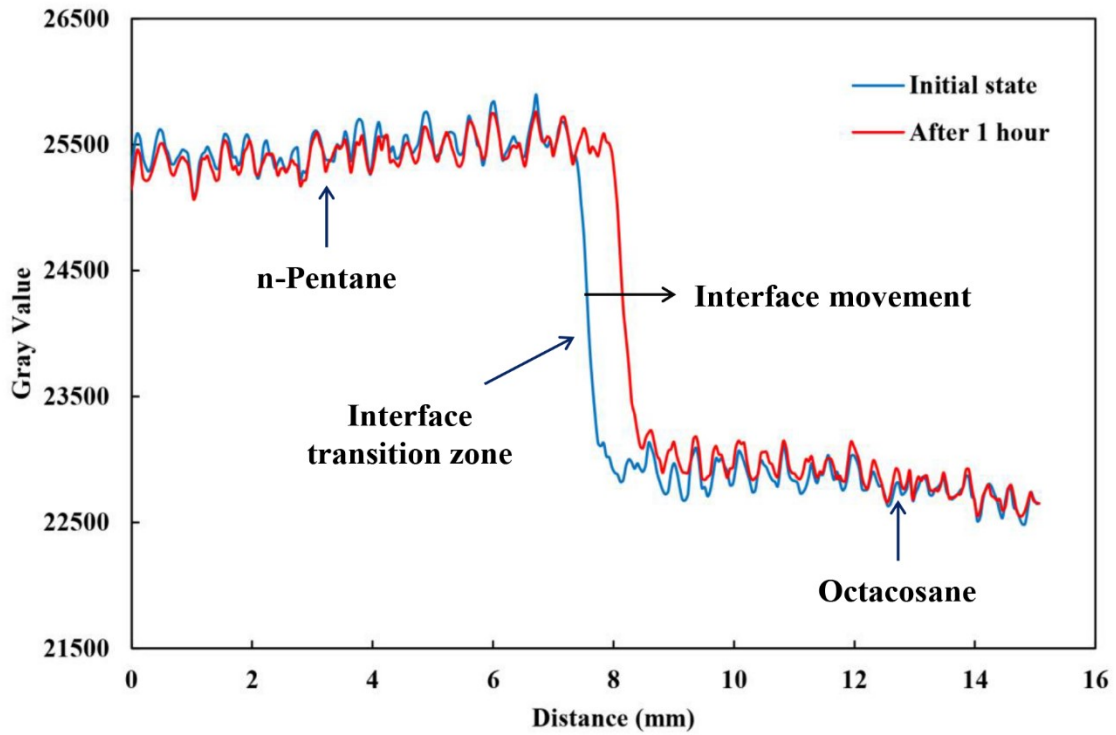


Figure 4-7. Intensity profiles of the areas of interest in the pentane-octacosane system in **Figure 4-6** with a horizontal interface (pentane below) at the initial state and 1 hour later.

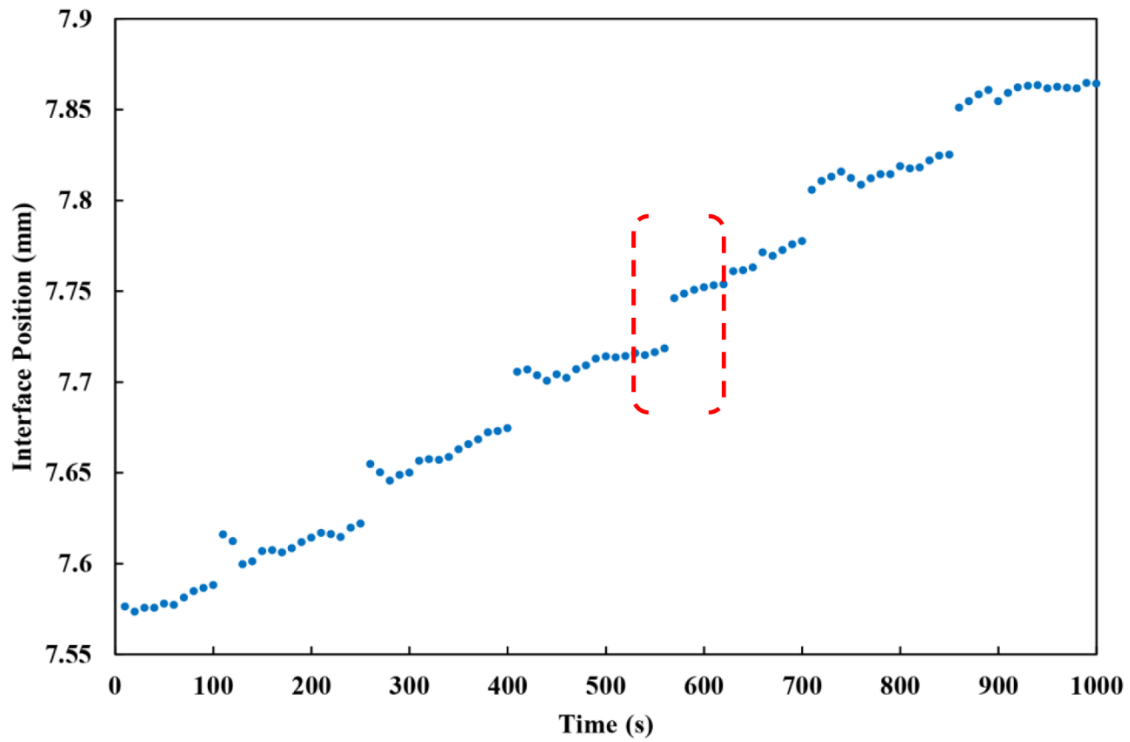


Figure 4-8. Interface displacement for the pentane-octacosane system with a horizontal interface (pentane below) from 0 to 1000 s.

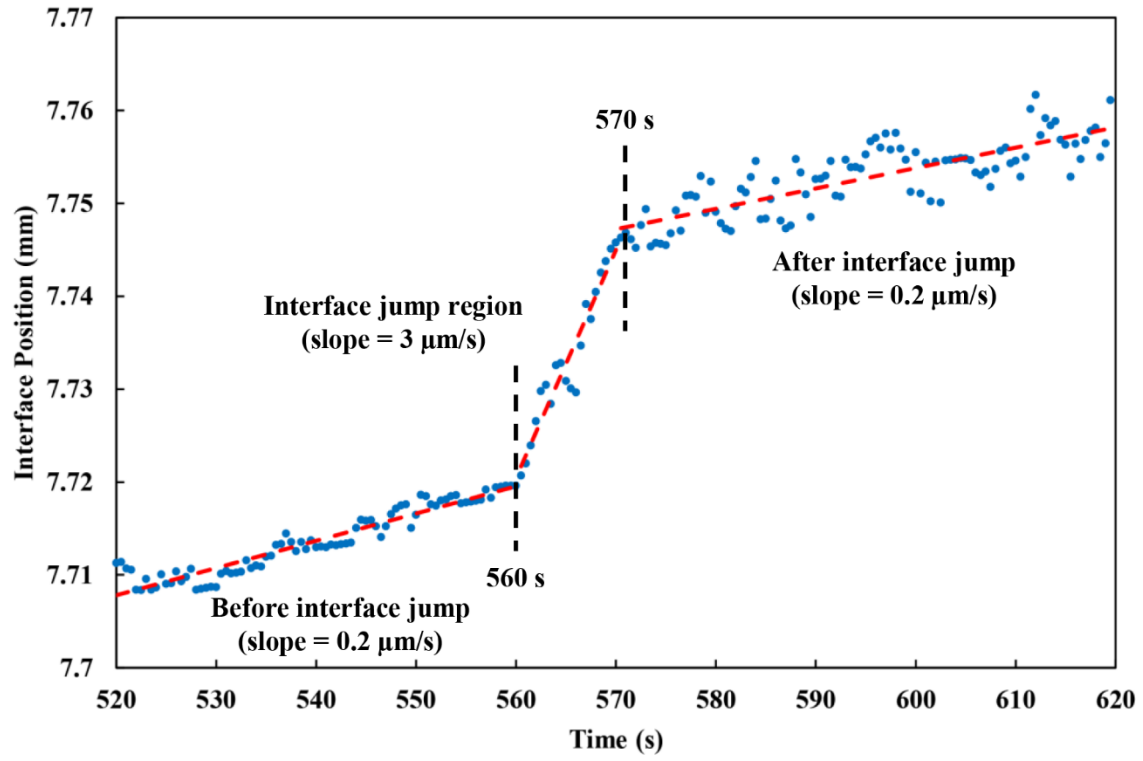


Figure 4-9. Interface displacement during the jump event from 520 s to 620 s highlighted with red dashed brackets in **Figure 4-8**.

4.5 Vertical Interface

For this case, we anticipate three effects based on the geometry. As the vial is on its side, the vertical dimension is limited to 2.5 cm at the central line of the vial. Fluids accumulating over time at the base of the interface are expected to inhibit fluid movement from the interface (during jumps and between jumps). Consequently, the driving force for interface displacement is expected to decrease over time and interface displacement is expected to be greater near the upper edge of the interface, and less at the lower edge of the interface.

Figure 4-10 shows the change of vertical pentane-octacosane interface in 1 hour. The glass vial is horizontally placed in the cabinet of the X-ray equipment. In this figure, the local angle (from the vertical) of the interface, near the top edge was initially 0° . It takes some time to seal the vial and place it in the X-ray cabinet. During this time, the angle increased to 4° . It increased further (to 10°) over one hour. The interface displacement to the right is also visibly greater near the upper edge than that at the lower edge of the interface.

From **Figure 4-11**, it is clear that the transmitted intensity of the pentane-rich phase decreases with time adjacent to the interface. This shows that the octacosane fraction in the liquid phase increases with time near the interface. This effect is present but less pronounced in **Figure 4-4** where little mass transfer occurs and is absent where fluid convects from the interface—**Figure 4-7**. As the octacosane content of the pentane adjacent to the interface increases, the driving force for mass transfer decreases. The quantitative interface displacement data, **Figure 4-12**, and the detailed analysis around an individual jump event, **Figure 4-13**, reflect these effects. Again, jump events arise every 150 s, but the magnitude of the events diminishes over time and the displacement rate

between jump events slows over time as well. For the jump event shown in **Figure 4-13**, the interface is displaced at $0.3 \mu\text{m/s}$ prior to the jump and $0.2 \mu\text{m/s}$ after the jump. During this jump event, the interface is displaced $36 \mu\text{m}$ over 6 s . The interface displacement rate, $6 \mu\text{m/s}$, during the jump event is one order of magnitude greater than the displacement rate between jump events and two orders of magnitude greater than the initial displacement rate for diffusive displacement. As long as the octacosane-enriched liquid drains away from the interface, an average displacement rate, over one cycle, $\sim 0.5 \mu\text{m/s}$ or 9 times of that achieved initially or 50 times the long-term displacement rate obtained for diffusion alone can be realized. If the octacosane-enriched liquid does not drain away from the interface, over time the displacement rate approaches the rate obtained for diffusion alone.

Figure 4-14 illustrates how the pentane-octacosane interface progresses during an interface disengagement event. The black grids represent pentane-heavy-blocks, while the white grids represent octacosane-heavy-blocks. The position of the interface is determined at the front black layer where more than half of the layer is filled with black grids. The yellow vertical line in each box shows the original interface position at 298.5 s . Before the interface jump, from 298.5 s to 300 s , there is no obvious interface displacement seen from these figures. The interface starts to jump at 300.5 s . It can be observed that half a layer of the black grids adds to the right of the interface indicating a sudden movement of the interface. The increase of the white grids in the pentane phase during the interface jump represents that the diluted octacosane moves from the octacosane body into the pentane phase. The interface jump accomplishes at the time of 306.5 s when almost a layer of black grids adds to the right. The diluted octacosane moves further into the pentane phase then drains down to the bottom of the glass vial due to gravity.

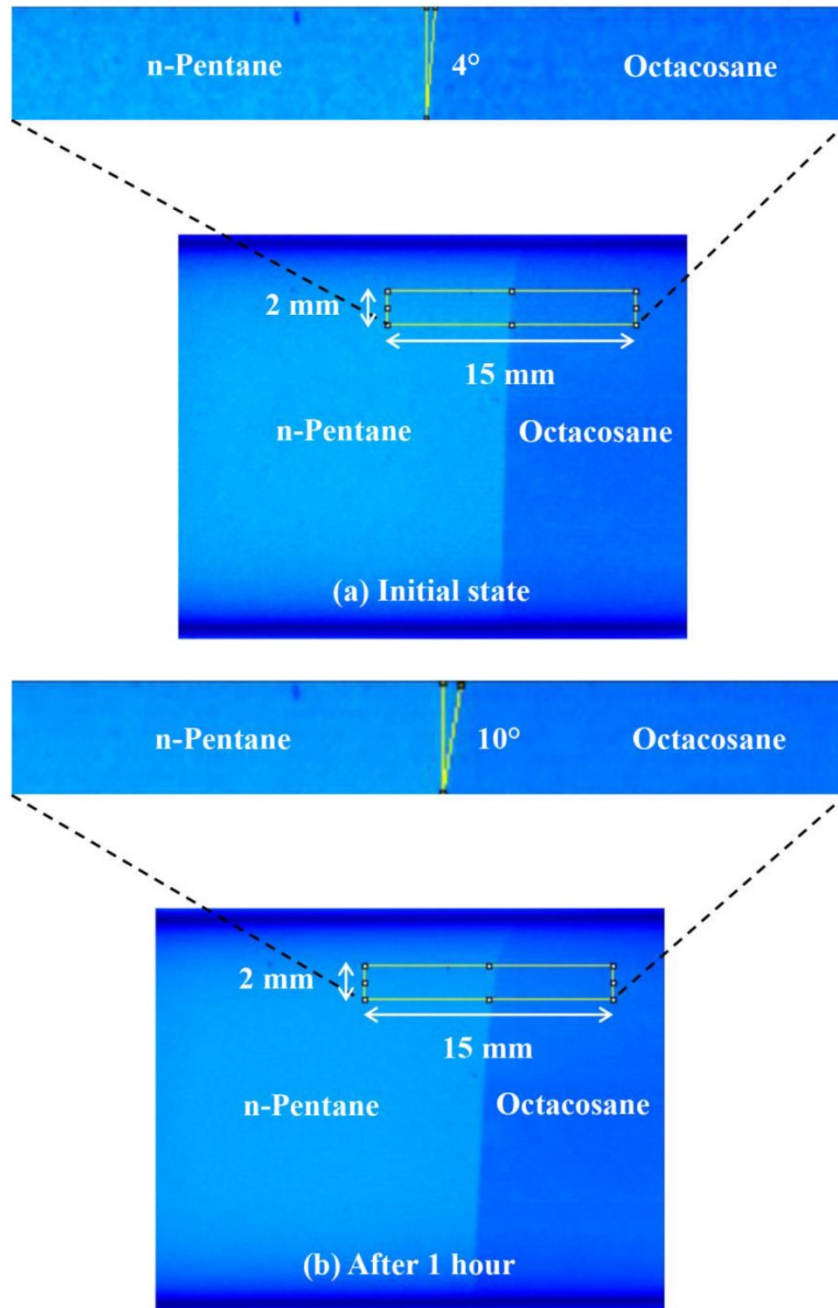


Figure 4-10. Images of the pentane-octacosane system with a vertical interface: (a) at the initial state and (b) 1 hour later.

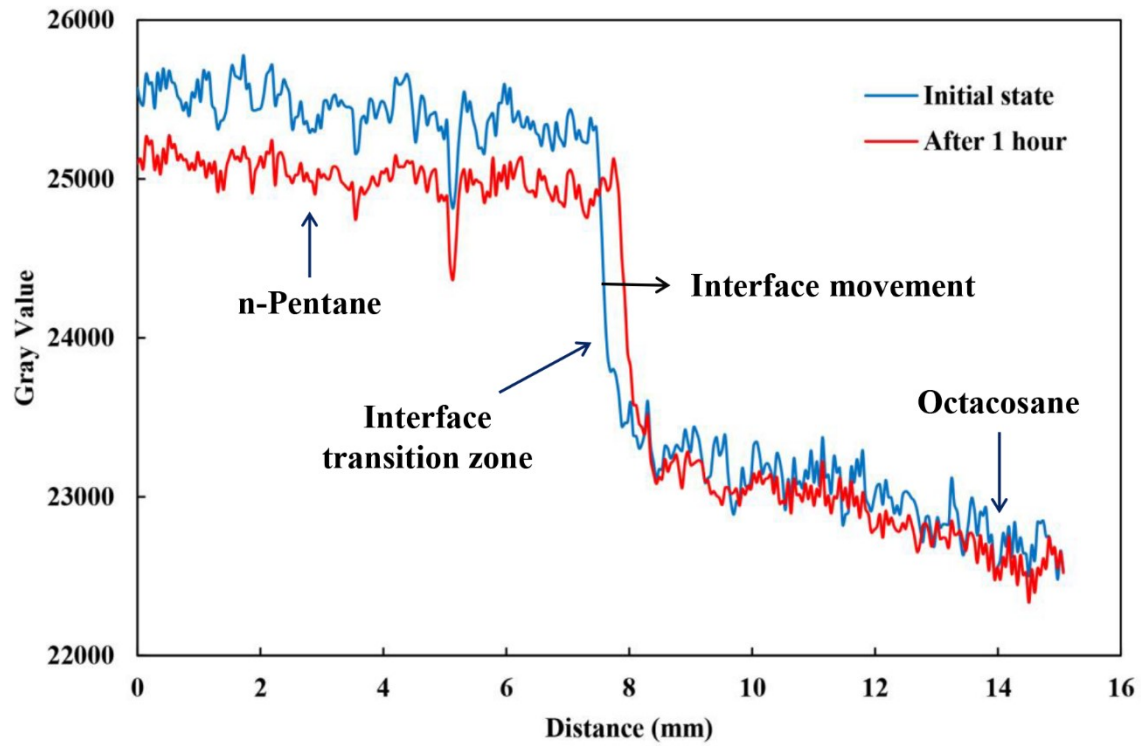


Figure 4-11. Intensity profiles of the area of interest in the pentane-octacosane system in **Figure 4-10**, vertical interface, at the initial state and 1 hour later.

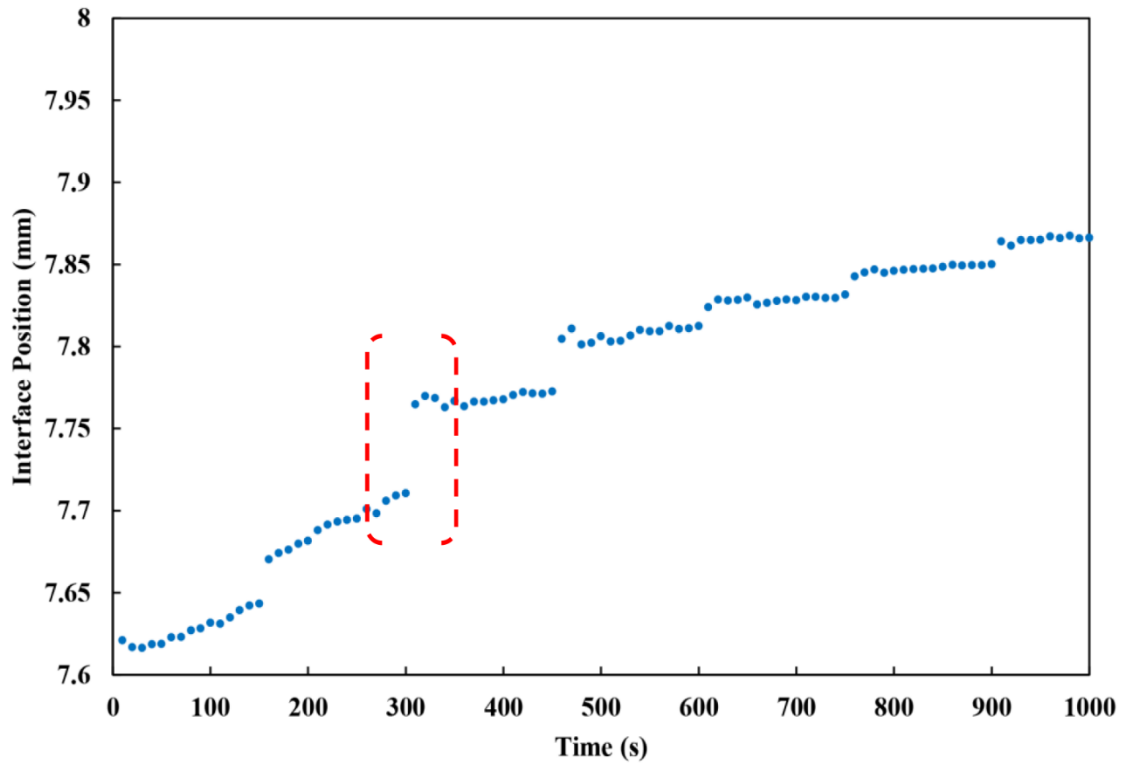


Figure 4-12. Interface displacement for the pentane-octacosane system with a vertical interface from 0 to 1000 s. The red dashed bracket area highlights the area analyzed in **Figure 4-13**.

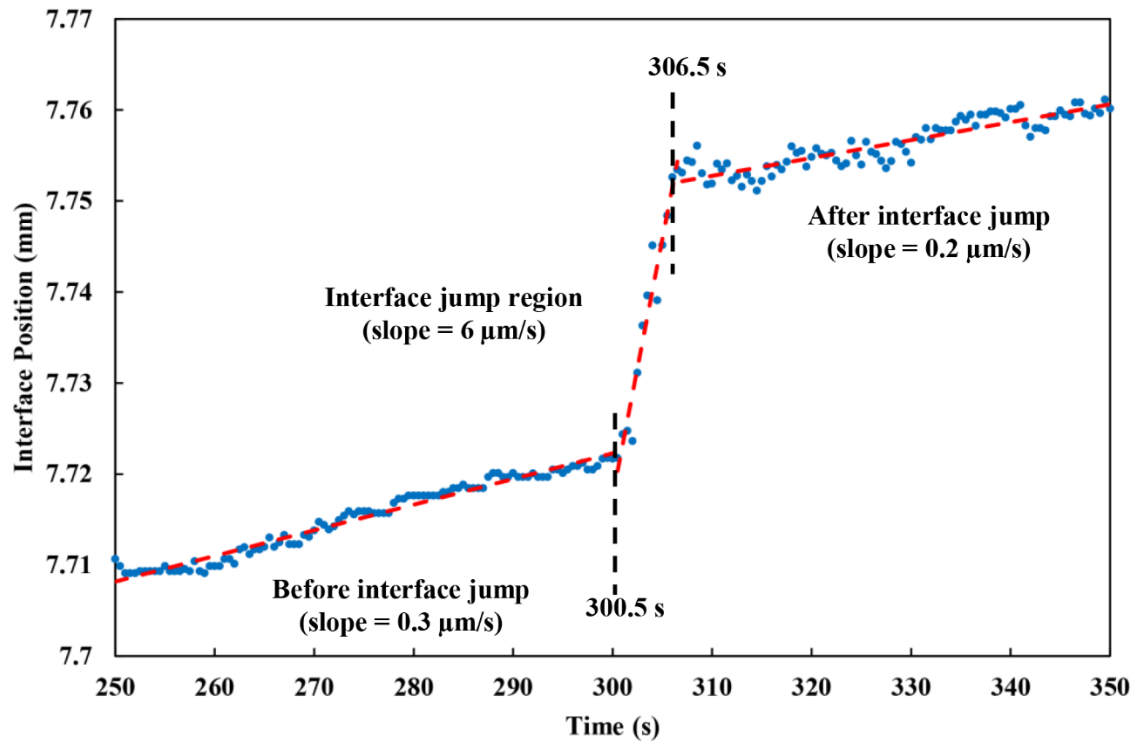


Figure 4-13. Interface displacement during the jump event from 250 s to 350 s highlighted with red dashed brackets in **Figure 4-12**.

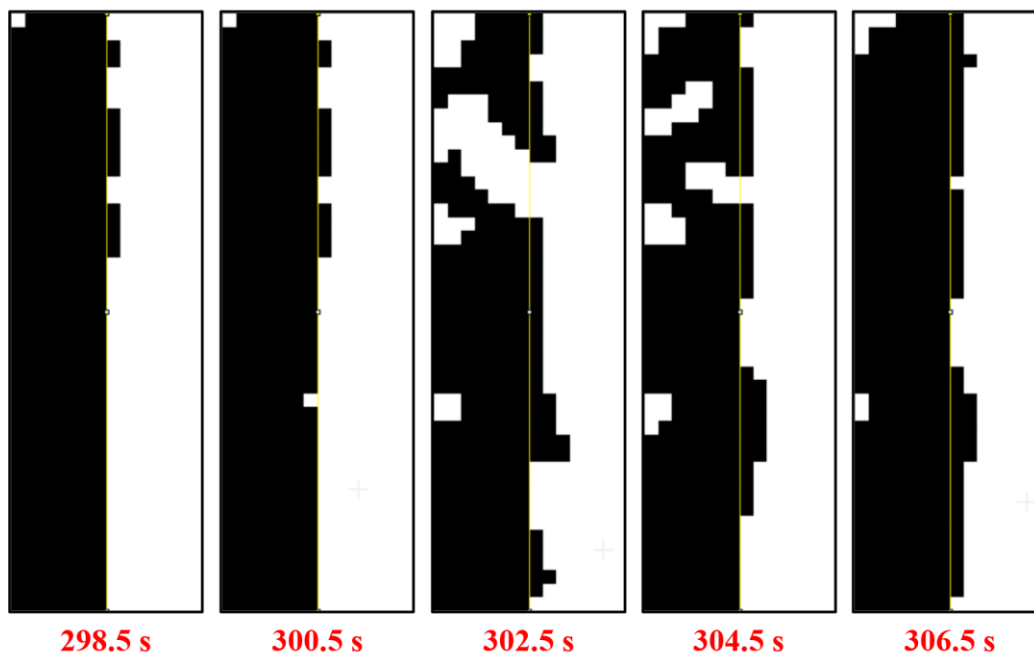


Figure 4-14. A sudden jump of the pentane-octacosane interface. The black grids represent pentane-heavy-blocks, while the white grids represent octacosane-heavy-blocks.

4.6 Summary

Table 4-1 summarizes interface progress rates of three different pentane-octacosane interface orientations. No interface disengagement behavior is observed for the case of horizontal interface with octacosane below. The average interface progress rate during the first 1000 second interval is $0.06 \mu\text{m/s}$. The expansion of the pentane diffusion layer leads to the average progress rate in 1-hour drops to $0.03 \mu\text{m/s}$. Our measurement results agree solvent penetrating bitumens rates ($\sim 0.01 \mu\text{m/s}$) (Tharanivasan et al., 2004; Zhang et al., 2007; Zhang and Shaw, 2007). Periodic interface disengagement events appear in both cases of horizontal interface with pentane below and vertical interface. For the earlier case, before reaching octacosane maximum solubility, the magnitude of jumps ($\sim 3 \mu\text{m/s}$) and interface progress rates between disengagement events ($\sim 0.2 \mu\text{m/s}$) do not vary much over 1000 seconds. Pentane-octacosane mixture with higher density travels to the bottom of the glass vial, which exposes “fresh” pentane to the pentane-octacosane interface maintaining a relatively high pentane diffusing rate. As of the case of vertical interface, pentane-octacosane interface displacement is episodic. Slow continuous penetration is interrupted by periodic short-duration interface jumps. The largest interface disengagement event ($\sim 6 \mu\text{m/s}$) occurs at the early stage of the solvent diffusion process. Due to the pentane-octacosane mixture builds up along vertical interface, the magnitude of jumps and progress rates between disengagement events ($\sim 0.3 \mu\text{m/s}$) gradually decreases over time.

Table 4-1. Summary of the interface progress rates

Interface orientation	Before interface jump ($\mu\text{m/s}$)	Between interface jump ($\mu\text{m/s}$)	After interface jump ($\mu\text{m/s}$)
Horizontal interface (pentane below)	0.2	3	0.2
Vertical interface	0.3	6	0.2
Horizontal Interface (octacosane below)	No interface jumps The average rate from 0 to 1000 seconds: $0.06 \mu\text{m/s}$		

4.7 Quantifying “Surface Renewal” or “Sloughing” Effects in Production Models

The experimental results highlight the impacts of interface orientation on the physics and chemistry and hence the rates of interface displacement arising over short time scales that impact long-term production rates, but which are not visible if displacement data are obtained at lower frequencies. It is only at these short time scales that “sloughing” and “surface renewal” effects are visible. Viewed from the perspective of time scales relevant to production schedules, these effects are appropriately averaged both with respect to time and the spatial orientation of interfaces. The duration of individual jump events (6 s to 10 s) and cycles between jump events (150 s) are orders of magnitude smaller than the time scales relevant to production. Our results do however provide a sound basis for establishing parameter values for production models. The parallels between our work and, for example, the solvent-based bitumen production experiments described by Das and Butler’s (Das and Butler, 1994a; Das and Butler, 1994b) are clear. For thin horizontal production

layers, vertical interfaces between solvent and unproduced reservoir fluid dominate. From our work, we anticipate sustained interface displacement rates of $\sim 0.5 \mu\text{m/s}$ as long as fluid disengages from the interface. If we use this value as the constant interface displacement rate and leave all other parameters in the Butler-Mokrys (Das and Butler, 1998) model unchanged, trends in production rate obtained from the experimental data of Das and Butler (Das and Butler, 1994a; Das and Butler, 1994b) are described semi-quantitatively over a broad range of permeabilities as illustrated in **Figure 4-15**. Heavy oil and bitumen formations often have permeabilities below this experimental range (1.2–7.5 Darcy) (James et al., 2007). At the length scales arising in small pores, additional or alternate physiochemical or fluid mechanics phenomena may dominate.

For next-generation production models, development of a clearer understanding of the roles of permeability on interface displacement is warranted, from theoretical and experimental perspectives. The dimensionless group analysis approach proposed by Stewart and Shaw (Stewart and Shaw, 2018), which focuses on the force balance and energy exchange within porous media on “sloughing”, may provide a suitable framework for concept and parameter development and assessment. Their approach emphasizes the importance of interfacial tension on bitumen production from porous media, i.e., a thin layer of diluted bitumen disengages from immobile bitumen when the gravitational force overcomes the interfacial force. They link “sloughing” in pores to the underlying mechanisms of “surface renewal” and “concentration shock”. Other approaches to understanding and quantifying interface displacement within hydrocarbon filled porous media are also tenable.

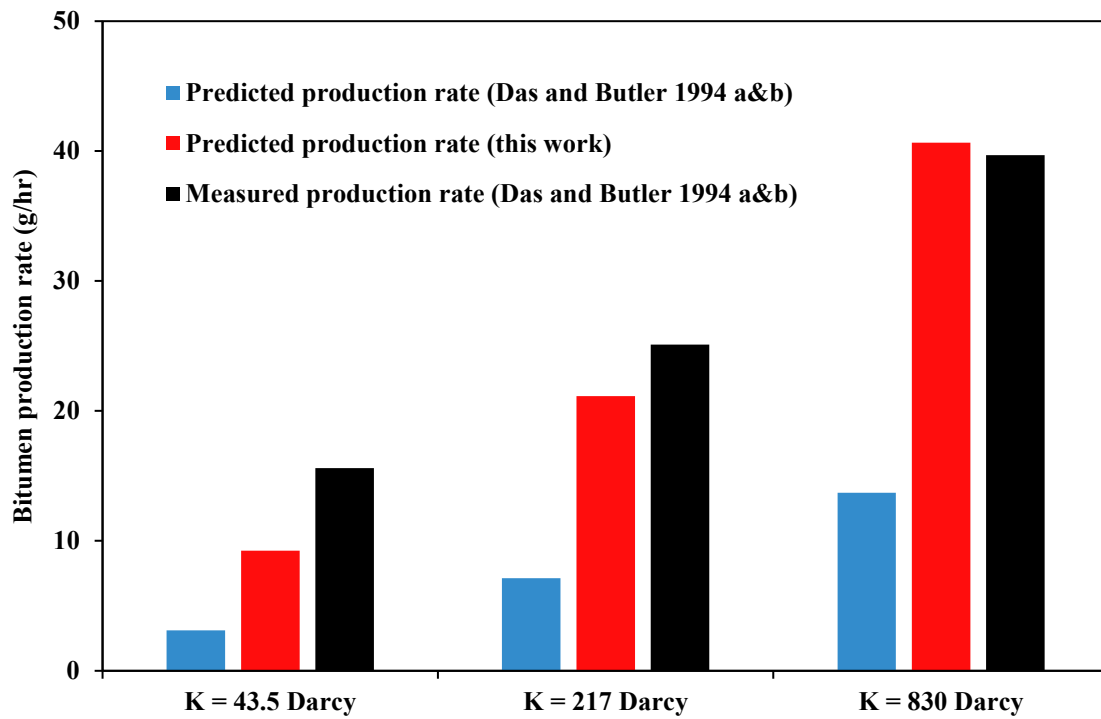


Figure 4-15. A comparison of predicted production rates using the Butler-Mokry's model and parameterized in this work with measured production rates (Das and Butler, 1994a; Das and Butler, 1994b).

CHAPTER 5 CONCLUSIONS AND RECOMMENDATIONS

5.1 Conclusions

The displacement of pentane-octacosane interfaces with varied orientations was evaluated over time using high spatial ($85\ \mu\text{m}$) and time ($0.033\ \text{s}$) resolution X-ray videography. For a horizontal interface with the octacosane below, interface displacement was driven by diffusion alone. Interface displacement was slow initially ($0.06\ \mu\text{m/s}$) and slowed to less than $0.03\ \mu\text{m/s}$ within one hour. For a vertical interface and a horizontal interface with pentane below, enhanced mass transfer effects were anticipated and were observed. Displacement of the interface occurred cyclically. Each cycle comprised a rapid steady displacement ($> 0.2\ \mu\text{m/s}$), relative to diffusive displacement, punctuated by an episodic jump event where a thin layer ($\sim 30\ \mu\text{m}$ thick) of octacosane-enriched pentane detached from the interface within $10\ \text{s}$. The jump events arose at $150\ \text{s}$ intervals and contributed approximately half of the overall displacement rate for each of these interface orientations. The overall displacement rates for these latter interface orientations were $0.5\ \mu\text{m/s}$ (vertical interface) and $0.4\ \mu\text{m/s}$ (horizontal interface pentane below).

These are the first direct measurements of “surface renewal” and “sloughing”, hypothesized explanations for the high production rates, relative to those anticipated from diffusion alone, observed for solvent-based production processes for heavy oils and bitumen irrespective of their scale. Direct use of the average interface displacement rate for vertical interfaces in the Butler-Mokrys, with other parameters unchanged, provided semi-quantitative agreement with laboratory-scale experimental production rate data for high permeability model reservoirs. For low

permeability porous media, interfacial phenomena are expected to play an important role and there is significant scope for additional theoretical and experimental contributions.

In many numerical simulation studies on solvent extraction processes, the solvent effective diffusivity rather than its molecular diffusivity measured based on Fick's law of diffusion is used. (Pourabdollah and Mokhtari, 2013). Assumed dispersion or diffusion coefficient which is often one to two orders of magnitude higher than the molecular diffusivity is used when doing history matching to match experimental results (Kapadia, 2004; Mohammadpoor and Torabi, 2015; Yazdani and Maini, 2008). However, higher dispersion coefficients associated with thicker solvent penetration depth (Das, 2005) contradicts with the experimental findings presented in this thesis—periodically renewed thin diffusion zone. In the numerical simulation study, periodic interface disengagement events should be included in the simulation processes. In addition, history matching should take account of the effect of “concentration shock” resulting from the “surface renewal” and “sloughing” discussed above. With regarding the porous media with low permeability, parameters such as capillary force and IFT should also be emphasized.

5.2 Recommendations

The research work presented above only covers a single pentane-octacosane system. To systematically study the mechanisms of solvent extraction processes, various vapor state or liquid state low carbon number alkanes ranging from C1 to C7 (Das, 1998) and different kinds of waxes such as hexacosane should be used to investigate the solvent-wax interface progression. It is anticipated that the solvent-wax interface progress rates and the frequencies of interface

disengagement events vary with different solvent-wax combinations. Further, a more complex liquid, bitumen should replace wax to study the solvent-bitumen fluid system. Asphaltene deposition may appear when the experimental pressure is close to the dew point pressure of vapor solvents (Das and Butler, 1994a). To fully mimic the real reservoir condition, interface progressions of solvent–wax or bitumen systems saturated in porous media at reservoir pressure and temperature should be investigated (Bayat et al., 2015). In presence of porous media, the IFT plays a significant role, and the “sloughing” phenomenon may be directly observed (Stewart and Shaw, 2018). Glass spheres or aluminum spheres, which are transparent to X-rays can be used to fabricate porous media (Al-Raoush and Willson, 2005; Reimann et al., 2017). Additionally, solvent–wax or bitumen interface progression in sand-packed porous media can be detected by using the acoustic cell (Di Pietro, 2018). A further experimental and theoretical study is required to understand and to quantify interfacial displacement effects in low permeability reservoirs (Thimm, 2007).

BIBLIOGRAPHY

- Al-Raoush, R. and Willson, C., 2005. Extraction of physically realistic pore network properties from three-dimensional synchrotron X-ray microtomography images of unconsolidated porous media systems. *Journal of hydrology*, 300(1-4): 44-64.
- Alberta Energy Regulator, 2019. Figure S3.1 Alberta crude bitumen production.
- Ardali, M., Mamora, D. and Barrufet, M.A., 2011. Experimental study of co-injection of potential solvents with steam to enhance SAGD process, SPE Western North American Region Meeting. Society of Petroleum Engineers.
- Argüelles-Vivas, F.J., Babadagli, T., Little, L., Romaniuk, N. and Ozum, B., 2012. High temperature density, viscosity, and interfacial tension measurements of bitumen–pentane–biodiesel and process water mixtures. *Journal of Chemical & Engineering Data*, 57(10): 2878-2889.
- Bayat, A.E., Junin, R., Hejri, S., Fazeli, A. and Afsari, K., 2015. Application of CO₂-based vapor extraction process for high pressure and temperature heavy oil reservoirs. *Journal of Petroleum Science and Engineering*, 135: 280-290.
- Bayestehparvin, B., Abedi, J. and Ali, S., 2015. Dissolution and Mobilization of Bitumen at Pore Scale, SPE Canada Heavy Oil Technical Conference. Society of Petroleum Engineers.
- Boberg, T.C., 1988. Thermal methods of oil recovery.
- Burgess, D., 2012. Thermochemical data. NIST Chemistry WebBook, NIST Standard Reference Database(69).
- Butler, R., Mokrys, I. and Herrera, P., 1985. Natural convection effects in the contacting of bitumen with diluents. *Aostr Journal of Research*, 2(3): 147-153.
- Chaar, M., Venetos, M., Dargin, J. and Palmer, D., 2015. Economics of steam generation for thermal enhanced oil recovery. *Oil and Gas Facilities*, 4(06): 42-50.

- Das, S., 2005. Diffusion and dispersion in the simulation of VAPEX process, SPE International Thermal Operations and Heavy Oil Symposium. Society of Petroleum Engineers.
- Das, S. and Butler, R., 1994a. Effect of asphaltene deposition on the Vapex process: A preliminary investigation using a Hele-Shaw cell. *Journal of Canadian Petroleum Technology*, 33(06).
- Das, S. and Butler, R., 1995. Extraction of heavy oil and bitumen using solvents at reservoir pressure, Technical meeting/petroleum conference of the South Saskatchewan section. Petroleum Society of Canada.
- Das, S.K., 1998. Vapex: An efficient process for the recovery of heavy oil and bitumen. *SPE journal*, 3(03): 232-237.
- Das, S.K. and Butler, R.M., 1994b. Investigation of " Vapex" Process in a Packed Cell Using Butane as a Solvent, SPE/CIM/CANMET International Conference on Recent Advances in Horizontal Well Applications. Petroleum Society of Canada.
- Das, S.K. and Butler, R.M., 1996. Diffusion coefficients of propane and butane in Peace River bitumen. *The Canadian journal of chemical engineering*, 74(6): 985-992.
- Das, S.K. and Butler, R.M., 1998. Mechanism of the vapor extraction process for heavy oil and bitumen. *Journal of Petroleum Science and Engineering*, 21(1-2): 43-59.
- Di Pietro, T., 2018. Mass transfer at an organic solid–organic liquid interface within reservoir rock under creeping flow conditions.
- Dini, Y., Becerra, M. and Shaw, J.M., 2016. Phase behavior and thermophysical properties of Peace River bitumen+ propane mixtures from 303 K to 393 K. *Journal of Chemical & Engineering Data*, 61(8): 2659-2668.
- Dorset, D.L., 2000. Chain length distribution and the lamellar crystal structure of a paraffin wax. *The Journal of Physical Chemistry B*, 104(35): 8346-8350.
- Dunn, S., Nenniger, E. and Rajan, V., 1989. A study of bitumen recovery by gravity drainage using low temperature soluble gas injection. *The Canadian Journal of Chemical Engineering*, 67(6): 978-991.

- Dusseault, M., 2001. Comparing Venezuelan and Canadian heavy oil and tar sands, Canadian international petroleum conference. Petroleum Society of Canada.
- Edmunds, N. and Gittins, S.D., 1993. Effective application of steam assisted gravity drainage of bitumen to long horizontal well pairs. *Journal of Canadian Petroleum Technology*, 32(06): 49-55.
- Gates, I. and Chakrabarty, N., 2006. Design of the steam and solvent injection strategy in expanding-solvent steam-assisted gravity drainage, Canadian international petroleum conference. Petroleum Society of Canada.
- Gates, I.D., 2010. Solvent-aided steam-assisted gravity drainage in thin oil sand reservoirs. *Journal of Petroleum Science and Engineering*, 74(3-4): 138-146.
- Hart, A., 2014. A review of technologies for transporting heavy crude oil and bitumen via pipelines. *Journal of Petroleum Exploration and Production Technology*, 4(3): 327-336.
- Haynes, W.M., 2016. *CRC Handbook of Chemistry and Physics*. CRC Press.
- He, L., Lin, F., Li, X., Xu, Z. and Sui, H., 2014. Enhancing bitumen liberation by controlling the interfacial tension and viscosity ratio through solvent addition. *Energy & fuels*, 28(12): 7403-7410.
- Hein, F.J., 2017. Geology of bitumen and heavy oil: An overview. *Journal of Petroleum Science and Engineering*, 154: 551-563.
- Irani, M. and Ghannadi, S., 2013. Understanding the heat-transfer mechanism in the steam-assisted gravity-drainage (SAGD) process and comparing the conduction and convection flux in bitumen reservoirs. *SPE Journal*, 18(01): 134-145.
- James, L., Rezaei, N. and Chatzis, I., 2007. VAPEX, Warm VAPEX, and Hybrid VAPEX-The State of Enhanced Oil Recovery for In Situ Heavy Oils in Canada, Canadian International Petroleum Conference. Petroleum Society of Canada.
- Jimenez, J., 2008. The field performance of SAGD projects in Canada, International petroleum technology conference. International Petroleum Technology Conference.

- Jyotsna, S. and Gates, I.D., 2010. Interfacial Stability and Displacement Efficiency in Thermal Solvent processes, SPE Improved Oil Recovery Symposium. Society of Petroleum Engineers.
- Kapadia, R.A., 2004. Dispersion determination in VAPEX: Experimental design, modeling and simulation, Masters Abstracts International.
- Leyva-Gomez, H. and Babadagli, T., 2016. Hot solvent injection for heavy oil/bitumen recovery from fractured reservoirs: An experimental approach to determine optimal application conditions. *Energy & Fuels*, 30(4): 2780-2790.
- Lin, L., 2014. Experimental, Theoretical, and Numerical Studies of Solvent-Based Heavy Oil Recovery Processes, Faculty of Graduate Studies and Research, University of Regina.
- Madsen, H.E.L. and Boistelle, R., 1976. Solubility of long-chain n-paraffins in pentane and heptane. *Journal of the Chemical Society, Faraday Transactions 1: Physical Chemistry in Condensed Phases*, 72(0): 1078-1081.
- Mohammadpoor, M. and Torabi, F., 2015. Comprehensive experimental study and numerical simulation of vapour extraction (VAPEX) process in heavy oil systems. *The Canadian Journal of Chemical Engineering*, 93(11): 1929-1940.
- Mokrys, I.J. and Butler, R.M., 1993. The rise of interfering solvent chambers: solvent analog model of steam-assisted gravity drainage. *Journal of Canadian Petroleum Technology*, 32(03).
- Mossop, G.D., 1980. Geology of the Athabasca oil sands. *Science*, 207(4427): 145-152.
- Naderi, K., Romaniuk, N., Little, L., Argüelles-Vivas, F. and Ozum, B., 2015. Effect of bitumen viscosity and bitumen–water interfacial tension on steam assisted bitumen recovery process efficiency. *Journal of Petroleum Science and Engineering*, 133: 862-868.
- Nasr, T.N. and Ayodele, O.R., 2006. New hybrid steam-solvent processes for the recovery of heavy oil and bitumen, Abu Dhabi International Petroleum Exhibition and Conference. Society of Petroleum Engineers.

- Nasr, T.N., Beaulieu, G., Golbeck, H. and Heck, G., 2003. Novel expanding solvent-SAGD process" ES-SAGD". *Journal of Canadian Petroleum Technology*, 42(01).
- Orr, B., 2009. ES-SAGD; past, present and future, SPE Annual Technical Conference and Exhibition. Society of Petroleum Engineers.
- Ovalles, C., 2019. *Subsurface Upgrading of Heavy Crude Oils and Bitumen*. CRC Press.
- Pathak, V., Babadagli, T. and Edmunds, N., 2011. Heavy oil and bitumen recovery by hot solvent injection. *Journal of petroleum science and engineering*, 78(3-4): 637-645.
- Pathak, V., Babadagli, T. and Edmunds, N., 2012. Mechanics of heavy-oil and bitumen recovery by hot solvent injection. *SPE Reservoir Evaluation & Engineering*, 15(02): 182-194.
- PetroWiki, 2020. Heavy oil.
- Pourabdollah, K. and Mokhtari, B., 2013. The VAPEX process, from beginning up to date. *Fuel*, 107: 1-33.
- Reimann, J. et al., 2017. X-ray tomography investigations of mono-sized sphere packing structures in cylindrical containers. *Powder Technology*, 318: 471-483.
- Rezaei, N., Mohammadzadeh, O. and Chatzis, I., 2010. Warm VAPEX: a thermally improved vapor extraction process for recovery of heavy oil and bitumen. *Energy & fuels*, 24(11): 5934-5946.
- Sadighian, A., Becerra, M., Bazyleva, A. and Shaw, J.M., 2011. Forced and diffusive mass transfer between pentane and Athabasca bitumen fractions. *Energy & Fuels*, 25(2): 782-790.
- Shah, A. et al., 2010. A review of novel techniques for heavy oil and bitumen extraction and upgrading. *Energy & Environmental Science*, 3(6): 700-714.
- Speight, J.G., 2014. *The chemistry and technology of petroleum*. CRC press.
- Stewart, R.A. and Shaw, J.M., 2018. Interface Renewal and Concentration Shock Through Sloughing: Accounting for the Dissonance Between Production Models and Measured Outcomes for Solvent-Assisted Bitumen-Production Processes. *SPE Reservoir Evaluation & Engineering*, 21(01): 174-186.

- Suranto, A., Bae, W. and Permadi, A., 2015. An investigation of hybrid steam-solvent injection for increasing economy and reducing CO₂ emission. *Petroleum Science and Technology*, 33(3): 302-310.
- Swenson, P., Tanchuk, B., Bastida, E., An, W. and Kuznicki, S.M., 2012. Water desalination and de-oiling with natural zeolite membranes—Potential application for purification of SAGD process water. *Desalination*, 286: 442-446.
- Tharanivasan, A.K., Yang, C. and Gu, Y., 2004. Comparison of three different interface mass transfer models used in the experimental measurement of solvent diffusivity in heavy oil. *Journal of Petroleum Science and Engineering*, 44(3-4): 269-282.
- Thimm, H., 2007. Permeability effects in a vapour extraction (VAPEX) heavy oil recovery process, Canadian International Petroleum Conference. Petroleum Society of Canada.
- Upreti, S., Lohi, A., Kapadia, R. and El-Haj, R., 2007. Vapor extraction of heavy oil and bitumen: a review. *Energy & Fuels*, 21(3): 1562-1574.
- Wang, T. et al., 2014. Solvent extraction of bitumen from oil sands. *Energy & fuels*, 28(4): 2297-2304.
- Wang, X., 2010. Experimental and numerical studies on multiple well pairs SAGD performance.
- White, P. and Moss, J.T., 1965. High-temperature thermal techniques for stimulating oil recovery. *Journal of Petroleum Technology*, 17(09): 1,007-1,011.
- Wu, C., De Visscher, A. and Gates, I.D., 2019. On naphthenic acids removal from crude oil and oil sands process-affected water. *Fuel*, 253: 1229-1246.
- Yang, C. and Gu, Y., 2005. Effects of heavy oil-solvent interfacial tension on gravity drainage in the vapor extraction (VAPEX) process, SPE International Thermal Operations and Heavy Oil Symposium. Society of Petroleum Engineers.
- Yazdani, A. and Maini, B.B., 2008. Modeling of the VAPEX process in a very large physical model. *Energy & Fuels*, 22(1): 535-544.
- Žbik, M., Horn, R.G. and Shaw, N., 2006. AFM study of paraffin wax surfaces. *Colloids and Surfaces A: Physicochemical and Engineering Aspects*, 287(1-3): 139-146.

- Zerkalov, G., 2015. Steam Injection for Enhanced Oil Recovery.
- Zhang, J. and Chen, Z., 2018. Formation Damage by Thermal Methods Applied to Heavy Oil Reservoirs, Formation Damage During Improved Oil Recovery. Elsevier, pp. 361-384.
- Zhang, X., Fulem, M. and Shaw, J.M., 2007. Liquid-phase mutual diffusion coefficients for athabasca bitumen+ pentane mixtures. Journal of Chemical & Engineering Data, 52(3): 691-694.
- Zhang, X. and Shaw, J., 2007. Liquid-phase mutual diffusion coefficients for heavy oil+ light hydrocarbon mixtures. Petroleum science and technology, 25(6): 773-790.

APPENDIX A: “EFFECTIVE DIFFUSIVITY” CALCULATION BASED ON DAS AND BUTLER’S EXPERIMENTAL RESULTS

The key factor brings dissonance between experimental production rates and predicted values based on Butler-Mokrys model is “ N_s ” as shown in equation [2-2]. More specifically, the intrinsic diffusivity of solvent in bitumen “ D_s ” involved in the calculation of “ N_s ” varies with reservoir condition. The effective diffusivity can be calculated based on data from Das and Butler’s experiments in systems of Lloydminster bitumen and vapor butane within porous media (sand-packed cell) (Das and Butler, 1994b).

In this experiment, the actual bitumen production rate “ Q ” is measured. The true value of “ N_s ” can be calculated as:

$$N_s = \frac{Q^2}{2kg\phi\Delta S_o h} \quad [\text{A-1}]$$

where, Q is the bitumen drainage rate (m^2/s); k is the Hele-Shaw cell permeability (cm^2); g is the gravitational acceleration (cm/hr^2); ϕ is the Hele-Shaw cell porosity; ΔS_o is the change in oil saturation; h is the height of the Hele-Shaw cell (cm).

The parameter “ N_s ” can also be expressed as (Das and Butler, 1998):

$$N_s = \int_{c_m}^{c_i} \frac{\Delta\rho D_s (1 - c_s)}{\mu c_s} dc_s \quad [\text{A-2}]$$

where, c_m is the minimum solvent volume concentration in solvent-bitumen mixture required to

mobilize; c_i is the solubility of solvent vapor in bitumen calculated by equation [A-3] (Das and Butler, 1996); c_s is the volume fraction of solvent in solvent-bitumen mixture; $\Delta\rho$ is the density difference between the diluted bitumen and pure solvent calculated by equation [A-4] (kg/m³) (Das and Butler, 1996); μ is the viscosity of diluted bitumen calculated by equation [A-5] (cP) (Mokrys and Butler, 1993); D_s is the intrinsic diffusivity of solvent in bitumen calculated by equation [A-6] (m²/s).

$$c_i = \frac{\frac{x_s}{\rho_s}}{\frac{1-x_s}{\rho_B} + \frac{x_s}{\rho_s}} \quad [\text{A-3}]$$

where, x_s is the solubility of butane vapor in bitumen (kg of butane/kg of diluted bitumen); ρ_s is the butane density (kg/m³); ρ_B is the bitumen viscosity (kg/m³).

$$\Delta\rho = c_s\rho_s + (1-c_s)\rho_B \quad [\text{A-4}]$$

$$\log \mu = 9.4686c_B^4 - 11.2857c_B^3 + 8.2544c_B^2 + 0.9303c_B - 0.1624 \quad [\text{A-5}]$$

where, c_B is the volume fraction of bitumen in solvent-bitumen mixture.

Assuming the intrinsic diffusivity of butane into bitumen increases linearly with its volume concentration. The butane intrinsic diffusivities are calculated as:

$$D_{S_{i+1}} = D_{S_i} + \alpha(c_{S_{i+1}} - c_{S_i}) \quad [\text{A-6}]$$

where, α is a scaling factor. The value of “ α ” is tuned until the value of “ N_s ” calculated by equation [A-2] equal to real value calculate by equation [A-1].

The values of parameters used for calculation are listed in **Table A-1**. The calculation results of butane “effective diffusivity” are listed in **Table A-2**.

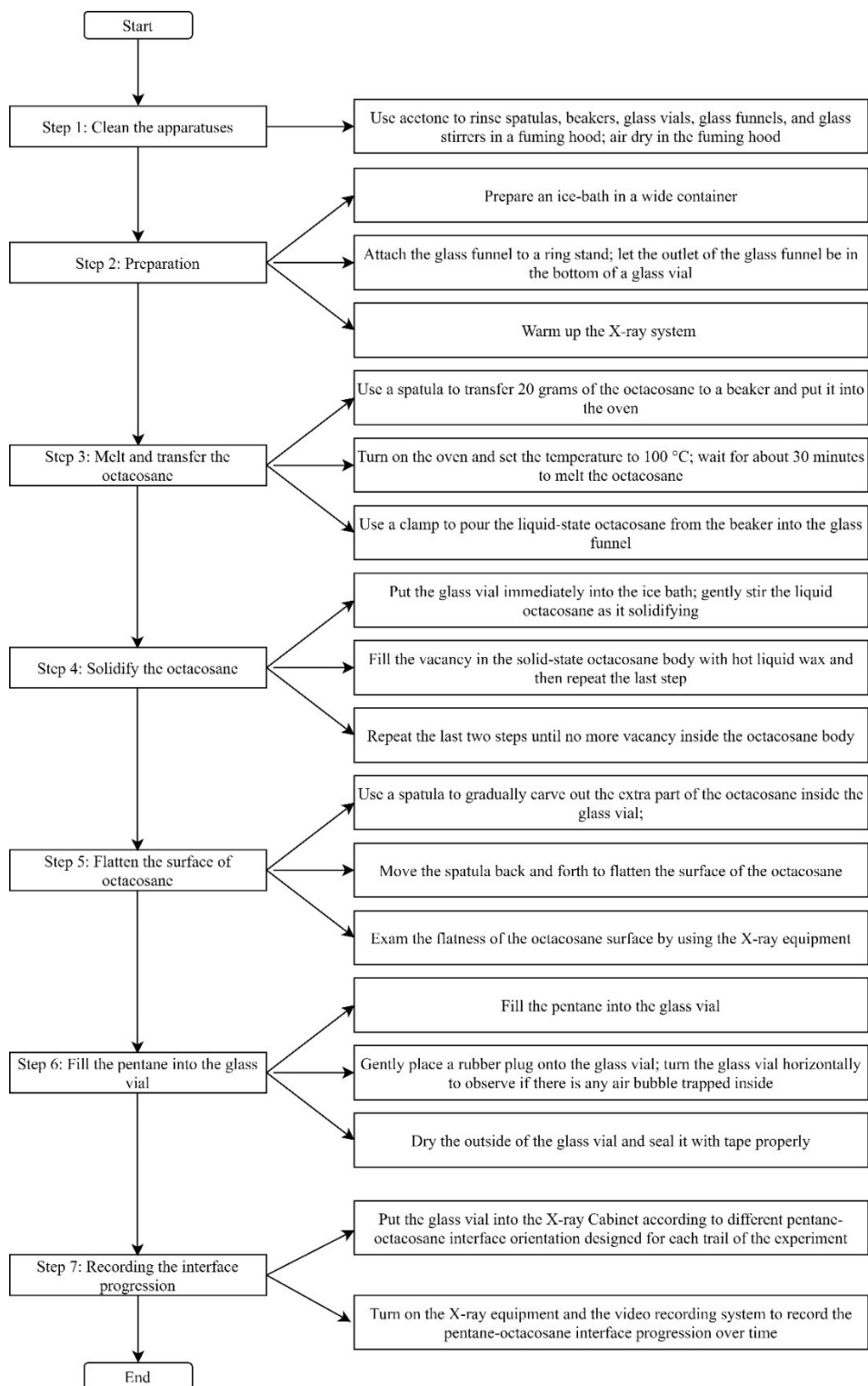
Table A-1. List of parameters for calculating butane “effective diffusivity”.

Parameter	Value	Assumption/Note
T	22 °C (Das and Butler, 1994b)	Experimental temperature
P	32.6 psia (Das and Butler, 1994b)	Vapor pressure of butane at experimental temperature
Q	13.23 cm ² /hr (Das and Butler, 1994b)	Bitumen production rate
k	830 Darcy (Das and Butler, 1994b)	Sand-pack cell permeability
ϕ	0.3	Assumed
ΔS_o	0.95	Assumed
h	21.9 cm (Das and Butler, 1994b)	Cell height
N_s	1.33×10^{-4}	True value
ρ_s	576.3 kg/m ³ (Burgess, 2012)	Butane density at experimental condition
ρ_B	1000 kg/m ³	Assumed
x_s	0.72 kg of butane/kg of oil mixture (Das and Butler, 1996)	Solubility of butane vapor in bitumen at 35°C and 0.334 MPa
c_m	0.01	Minimum butane volume concentration
c_i	0.817 (Das and Butler, 1996)	Solubility of solvent vapor in bitumen
D_s	1×10^{-6} cm ² /s (Das and Butler, 1996)	Butane intrinsic diffusivity at c_m
α	9.69×10^{-7}	Tuned value

Table A-2. Summary of variables at different butane volume concentration.

c_s	$\Delta\rho$ (kg/m^3)	μ (cP)	D_s (cm^2/s)	c_s	$\Delta\rho$ (kg/m^3)	μ (cP)	D_s (cm^2/s)
0.01	995.8	9817115	1.00E-10	0.42	822	105.5	3.97E-07
0.02	991.5	6118574	9.79E-09	0.43	817.8	91	4.07E-07
0.03	987.3	3865832	1.95E-08	0.44	813.6	78.7	4.17E-07
0.04	983.1	2475189	2.92E-08	0.45	809.3	68.3	4.26E-07
0.05	978.8	1605442	3.89E-08	0.46	805.1	59.5	4.36E-07
0.06	974.6	1054515	4.85E-08	0.47	800.9	52	4.46E-07
0.07	970.3	701189.2	5.82E-08	0.48	796.6	45.6	4.56E-07
0.08	966.1	471843.2	6.79E-08	0.49	792.4	40	4.65E-07
0.09	961.9	321216.4	7.76E-08	0.5	788.2	35.3	4.75E-07
0.1	957.6	221154.1	8.73E-08	0.51	783.9	31.1	4.85E-07
0.11	953.4	153940	9.70E-08	0.52	779.7	27.6	4.94E-07
0.12	949.2	108300.8	1.07E-07	0.53	775.4	24.5	5.04E-07
0.13	944.9	76984.3	1.16E-07	0.54	771.2	21.7	5.14E-07
0.14	940.7	55275.4	1.26E-07	0.55	767	19.4	5.23E-07
0.15	936.4	40076.7	1.36E-07	0.56	762.7	17.3	5.33E-07
0.16	932.2	29332.9	1.45E-07	0.57	758.5	15.5	5.43E-07
0.17	928	21667	1.55E-07	0.58	754.3	13.9	5.52E-07
0.18	923.7	16147.2	1.65E-07	0.59	750	12.5	5.62E-07
0.19	919.5	12137.7	1.75E-07	0.6	745.8	11.2	5.72E-07
0.2	915.3	9200.1	1.84E-07	0.61	741.5	10.1	5.81E-07
0.21	911	7030	1.94E-07	0.62	737.3	9.1	5.91E-07
0.22	906.8	5413.9	2.04E-07	0.63	733.1	8.3	6.01E-07
0.23	902.5	4201	2.13E-07	0.64	728.8	7.5	6.11E-07
0.24	898.3	3283.7	2.23E-07	0.65	724.6	6.8	6.20E-07
0.25	894.1	2584.8	2.33E-07	0.66	720.4	6.2	6.30E-07
0.26	889.8	2048.7	2.42E-07	0.67	716.1	5.6	6.40E-07
0.27	885.6	1634.5	2.52E-07	0.68	711.9	5.1	6.49E-07
0.28	881.4	1312.3	2.62E-07	0.69	707.6	4.7	6.59E-07
0.29	877.1	1060.1	2.71E-07	0.7	703.4	4.3	6.69E-07
0.3	872.9	861.5	2.81E-07	0.71	699.2	3.9	6.78E-07
0.31	868.7	704.1	2.91E-07	0.72	694.9	3.6	6.88E-07
0.32	864.4	578.6	3.00E-07	0.73	690.7	3.3	6.98E-07
0.33	860.2	478	3.10E-07	0.74	686.5	3	7.07E-07
0.34	855.9	397	3.20E-07	0.75	682.2	2.8	7.17E-07
0.35	851.7	331.2	3.30E-07	0.76	678	2.6	7.27E-07
0.36	847.5	277.7	3.39E-07	0.77	673.8	2.4	7.37E-07
0.37	843.2	233.9	3.49E-07	0.78	669.5	2.2	7.46E-07
0.38	839	197.9	3.59E-07	0.79	665.3	2	7.56E-07
0.39	834.8	168.1	3.68E-07	0.8	661	1.9	7.66E-07
0.4	830.5	143.3	3.78E-07	0.81	656.8	1.8	7.75E-07
0.41	826.3	122.7	3.88E-07	0.82	653.9	1.7	7.85E-07

APPENDIX B: FLOWCHART OF EXPERIMENTAL PROCEDURES



APPENDIX C: EXPERIMENTAL DATA OF THE VERTICAL PENTANE-OCTACOSANE INTERFACE SCENARIO

Table C-1. Intensity data from 0 to 100 seconds.

Position (mm)	Gray Values										
	0 s	10 s	20 s	30 s	40 s	50 s	60 s	70 s	80 s	90 s	100 s
0.000	25570	25625	25625	25604	25590	25604	25570	25584	25577	25584	25563
0.047	25487	25556	25632	25570	25590	25597	25590	25590	25604	25577	25563
0.093	25466	25487	25549	25570	25570	25590	25556	25570	25590	25563	25556
0.140	25660	25653	25708	25715	25694	25687	25701	25701	25715	25694	25674
0.187	25597	25535	25570	25570	25556	25549	25535	25535	25542	25535	25521
0.233	25604	25570	25570	25577	25577	25583	25577	25563	25570	25563	25563
0.280	25445	25459	25452	25473	25431	25431	25417	25404	25417	25431	25431
0.326	25667	25674	25611	25611	25570	25549	25528	25542	25556	25570	25556
0.373	25556	25597	25500	25528	25466	25459	25438	25424	25424	25424	25417
0.420	25695	25708	25660	25639	25611	25556	25556	25535	25535	25535	25501
0.466	25570	25556	25535	25542	25487	25494	25501	25494	25494	25500	25487
0.513	25681	25667	25639	25639	25639	25674	25667	25646	25674	25667	25674
0.560	25611	25618	25584	25597	25591	25597	25618	25632	25632	25611	25611
0.606	25598	25611	25625	25653	25660	25688	25701	25715	25688	25667	25674
0.653	25521	25556	25597	25625	25618	25625	25618	25604	25611	25597	25618
0.700	25494	25556	25584	25591	25597	25584	25591	25570	25591	25577	25577
0.746	25431	25480	25466	25480	25514	25487	25466	25466	25487	25480	25466
0.793	25480	25445	25473	25473	25466	25473	25438	25424	25459	25445	25438
0.840	25397	25355	25383	25320	25348	25362	25369	25348	25348	25348	25362
0.886	25542	25487	25507	25473	25480	25473	25487	25494	25487	25500	25473
0.933	25514	25500	25542	25528	25535	25507	25507	25528	25494	25494	25500
0.979	25625	25681	25687	25667	25674	25687	25653	25674	25653	25687	25667
1.026	25487	25514	25480	25514	25501	25514	25500	25514	25514	25535	25521
1.073	25680	25570	25549	25591	25563	25563	25590	25584	25570	25563	25556
1.119	25625	25473	25473	25452	25410	25445	25452	25466	25452	25431	25459
1.166	25667	25563	25556	25528	25500	25507	25528	25521	25542	25521	25528
1.213	25466	25445	25480	25500	25452	25452	25452	25452	25459	25445	25431
1.259	25438	25563	25577	25549	25521	25528	25556	25542	25535	25535	25542
1.306	25313	25390	25355	25313	25327	25334	25341	25355	25348	25341	25341
1.353	25362	25417	25445	25452	25424	25424	25459	25445	25445	25445	25431
1.399	25376	25410	25410	25410	25438	25417	25397	25397	25383	25397	25376
1.446	25438	25487	25480	25507	25480	25466	25473	25473	25466	25473	25487
1.493	25591	25570	25521	25542	25570	25535	25535	25521	25521	25514	25528

Position (mm)	Gray Values										
	0 s	10 s	20 s	30 s	40 s	50 s	60 s	70 s	80 s	90 s	100 s
1.539	25715	25681	25611	25632	25653	25646	25604	25591	25597	25591	25584
1.586	25653	25618	25639	25584	25597	25618	25584	25590	25577	25577	25577
1.632	25639	25611	25653	25563	25570	25549	25528	25542	25563	25556	25549
1.679	25632	25646	25611	25577	25556	25570	25542	25549	25570	25556	25563
1.726	25778	25764	25743	25681	25681	25701	25687	25660	25653	25660	25667
1.772	25570	25611	25639	25604	25597	25597	25556	25577	25563	25597	25590
1.819	25597	25591	25604	25584	25570	25570	25570	25542	25535	25528	25556
1.866	25438	25334	25313	25341	25341	25348	25348	25327	25334	25320	25334
1.912	25431	25341	25369	25396	25403	25417	25445	25445	25452	25445	25431
1.959	25438	25369	25438	25459	25480	25459	25480	25480	25466	25473	25473
2.006	25445	25452	25473	25459	25473	25466	25507	25501	25494	25500	25487
2.052	25521	25466	25487	25494	25466	25466	25445	25438	25424	25417	25431
2.099	25653	25667	25687	25674	25653	25646	25639	25604	25577	25563	25584
2.146	25681	25680	25660	25625	25632	25604	25584	25577	25556	25542	25549
2.192	25715	25687	25646	25639	25639	25646	25618	25604	25597	25618	25611
2.239	25466	25390	25376	25403	25383	25403	25383	25390	25383	25397	25403
2.285	25528	25493	25521	25535	25528	25528	25528	25535	25521	25535	25521
2.332	25535	25480	25521	25521	25500	25514	25542	25535	25507	25521	25535
2.379	25625	25528	25556	25542	25542	25549	25542	25542	25556	25535	25521
2.425	25584	25556	25521	25549	25542	25521	25535	25514	25521	25507	25494
2.472	25535	25563	25556	25577	25577	25549	25570	25577	25563	25528	25528
2.519	25313	25355	25362	25348	25355	25334	25355	25362	25341	25362	25355
2.565	25383	25411	25397	25404	25383	25348	25355	25369	25383	25390	25390
2.612	25397	25466	25466	25480	25431	25417	25417	25404	25390	25404	25417
2.659	25487	25521	25480	25466	25466	25459	25473	25445	25445	25452	25452
2.705	25348	25438	25376	25417	25417	25397	25404	25390	25369	25404	25404
2.752	25362	25459	25445	25480	25445	25459	25459	25431	25452	25459	25452
2.799	25293	25403	25417	25376	25397	25431	25404	25417	25417	25424	25417
2.845	25313	25397	25390	25397	25397	25404	25390	25397	25404	25404	25390
2.892	25300	25327	25320	25279	25314	25341	25348	25355	25348	25362	25362
2.938	25404	25459	25494	25445	25459	25473	25480	25466	25438	25480	25487
2.985	25320	25341	25390	25383	25417	25445	25404	25383	25390	25383	25390
3.032	25487	25424	25410	25417	25438	25459	25452	25424	25445	25459	25459
3.078	25494	25410	25397	25404	25404	25417	25397	25397	25417	25438	25424
3.125	25438	25452	25507	25466	25459	25445	25424	25404	25397	25397	25404
3.172	25508	25480	25528	25501	25507	25501	25487	25473	25494	25487	25487
3.218	25528	25459	25521	25466	25480	25500	25500	25494	25487	25507	25494
3.265	25459	25369	25397	25438	25424	25431	25445	25431	25424	25431	25417
3.312	25494	25438	25466	25480	25424	25417	25410	25431	25424	25452	25452
3.358	25466	25570	25563	25563	25507	25521	25500	25500	25500	25480	25494
3.405	25452	25521	25500	25507	25500	25507	25480	25466	25445	25438	25410
3.451	25452	25445	25424	25417	25438	25417	25445	25438	25404	25411	25390

Position (mm)	Gray Values										
	0 s	10 s	20 s	30 s	40 s	50 s	60 s	70 s	80 s	90 s	100 s
3.498	25431	25355	25390	25404	25390	25383	25390	25390	25390	25404	25397
3.545	25161	25147	25175	25203	25203	25133	25161	25175	25161	25161	25161
3.591	25182	25223	25272	25272	25244	25210	25244	25244	25230	25237	25237
3.638	25369	25397	25431	25404	25376	25355	25341	25348	25341	25334	25334
3.685	25397	25466	25383	25348	25334	25334	25320	25320	25307	25293	25313
3.731	25355	25445	25334	25334	25376	25376	25362	25334	25355	25348	25341
3.778	25501	25521	25424	25410	25438	25466	25452	25431	25404	25403	25404
3.825	25487	25473	25445	25424	25431	25459	25445	25438	25431	25431	25445
3.871	25383	25383	25383	25369	25355	25397	25397	25397	25410	25390	25383
3.918	25431	25417	25417	25383	25376	25404	25410	25404	25410	25397	25390
3.965	25487	25480	25521	25528	25487	25507	25521	25521	25521	25514	25507
4.011	25480	25549	25521	25514	25452	25466	25507	25494	25494	25500	25507
4.058	25424	25514	25514	25494	25438	25452	25452	25431	25431	25431	25438
4.104	25355	25424	25438	25417	25383	25369	25410	25355	25341	25341	25355
4.151	25431	25480	25473	25459	25424	25403	25417	25369	25403	25417	25410
4.198	25632	25632	25618	25625	25591	25549	25549	25535	25549	25556	25570
4.244	25597	25542	25542	25549	25514	25521	25507	25535	25514	25514	25521
4.291	25597	25563	25500	25507	25507	25480	25480	25494	25493	25480	25466
4.338	25625	25549	25501	25514	25508	25473	25494	25473	25487	25508	25494
4.384	25660	25521	25494	25494	25514	25535	25507	25521	25521	25542	25535
4.431	25597	25521	25466	25494	25500	25500	25473	25487	25514	25507	25514
4.478	25424	25466	25417	25424	25424	25424	25424	25424	25424	25445	25473
4.524	25230	25306	25251	25286	25286	25313	25313	25313	25293	25313	25327
4.571	25369	25424	25369	25411	25410	25417	25424	25431	25411	25390	25404
4.618	25521	25480	25459	25507	25494	25459	25487	25466	25452	25452	25424
4.664	25494	25459	25390	25438	25445	25376	25390	25397	25410	25424	25397
4.711	25341	25320	25314	25327	25327	25293	25286	25314	25307	25320	25314
4.757	25397	25445	25410	25410	25424	25404	25397	25424	25424	25410	25403
4.804	25410	25452	25445	25445	25410	25431	25445	25452	25424	25431	25410
4.851	25417	25445	25404	25404	25390	25438	25438	25452	25431	25424	25424
4.897	25307	25258	25230	25210	25237	25272	25272	25279	25272	25272	25286
4.944	25327	25286	25279	25279	25293	25279	25327	25327	25327	25341	25341
4.991	25251	25272	25286	25307	25272	25279	25307	25293	25300	25293	25300
5.037	25362	25355	25341	25348	25334	25307	25334	25341	25348	25355	25369
5.084	24932	24925	24919	24919	24912	24905	24925	24953	24939	24925	24932
5.131	24815	24766	24780	24780	24780	24801	24787	24815	24815	24801	24822
5.177	24932	24960	24960	24960	24967	24939	24953	24953	24953	24953	24953
5.224	25216	25293	25300	25286	25272	25258	25258	25258	25293	25300	25293
5.271	25417	25507	25494	25480	25494	25494	25507	25480	25473	25473	25459
5.317	25549	25521	25528	25480	25500	25514	25494	25494	25501	25480	25507
5.364	25424	25369	25369	25327	25341	25362	25348	25341	25348	25355	25341
5.410	25487	25487	25494	25445	25473	25487	25480	25500	25480	25445	25459

Position (mm)	Gray Values										
	0 s	10 s	20 s	30 s	40 s	50 s	60 s	70 s	80 s	90 s	100 s
5.457	25376	25334	25348	25362	25355	25341	25341	25355	25348	25320	25341
5.504	25307	25279	25327	25320	25327	25334	25355	25362	25355	25334	25348
5.550	25196	25203	25300	25286	25314	25327	25307	25314	25314	25314	25314
5.597	25196	25279	25348	25313	25341	25390	25376	25390	25383	25369	25362
5.644	25161	25217	25286	25272	25293	25313	25369	25362	25369	25341	25334
5.690	25348	25355	25390	25397	25390	25390	25376	25390	25390	25410	25424
5.737	25390	25327	25424	25362	25369	25369	25341	25334	25334	25327	25348
5.784	25410	25500	25521	25521	25521	25507	25494	25500	25507	25500	25521
5.830	25272	25286	25293	25313	25293	25313	25313	25327	25320	25334	25334
5.877	25473	25466	25459	25424	25459	25473	25445	25459	25473	25480	25459
5.924	25480	25404	25390	25410	25404	25410	25417	25424	25397	25403	25397
5.970	25597	25535	25507	25501	25501	25514	25501	25494	25480	25473	25487
6.017	25473	25376	25362	25341	25341	25320	25314	25334	25334	25341	25348
6.063	25570	25577	25528	25500	25500	25487	25487	25487	25487	25487	25487
6.110	25362	25431	25424	25348	25355	25362	25355	25376	25376	25362	25383
6.157	25383	25459	25459	25438	25431	25431	25466	25473	25459	25459	25487
6.203	25424	25487	25521	25480	25480	25507	25542	25542	25549	25563	25542
6.250	25334	25390	25417	25424	25424	25480	25500	25500	25507	25521	25507
6.297	25327	25341	25355	25376	25369	25410	25403	25410	25417	25431	25417
6.343	25390	25424	25417	25417	25376	25403	25397	25383	25410	25410	25397
6.390	25314	25348	25341	25341	25334	25348	25362	25383	25348	25383	25383
6.437	25362	25348	25383	25355	25307	25327	25348	25362	25376	25397	25376
6.483	25293	25341	25362	25327	25286	25300	25320	25341	25334	25327	25307
6.530	25272	25424	25431	25445	25452	25452	25466	25500	25487	25494	25480
6.576	25210	25320	25334	25355	25383	25397	25403	25410	25397	25390	25404
6.623	25334	25327	25334	25362	25383	25369	25341	25341	25348	25348	25362
6.670	25341	25279	25279	25300	25272	25279	25258	25279	25244	25272	25272
6.716	25244	25293	25237	25272	25272	25258	25258	25258	25286	25279	25258
6.763	25182	25272	25230	25272	25244	25230	25237	25251	25244	25217	25217
6.810	25355	25348	25341	25362	25362	25334	25341	25348	25369	25355	25334
6.856	25272	25258	25265	25300	25251	25272	25258	25272	25272	25258	25265
6.903	25237	25251	25251	25244	25237	25244	25244	25223	25244	25244	25237
6.950	25210	25210	25265	25210	25251	25251	25265	25265	25258	25237	25230
6.996	25390	25390	25383	25403	25417	25417	25417	25383	25397	25397	25383
7.043	25438	25431	25493	25494	25507	25480	25459	25445	25452	25459	25445
7.090	25383	25341	25431	25417	25424	25376	25369	25362	25355	25320	25320
7.136	25251	25223	25293	25258	25237	25244	25265	25237	25265	25265	25265
7.183	25307	25265	25293	25293	25320	25314	25334	25314	25320	25313	25327
7.229	25244	25168	25203	25182	25224	25203	25217	25224	25251	25224	25237
7.276	25230	25154	25140	25133	25189	25175	25196	25140	25154	25133	25147
7.323	25230	25244	25161	25175	25182	25182	25175	25161	25161	25168	25182
7.369	25383	25334	25314	25320	25314	25320	25320	25279	25286	25279	25286

Position (mm)	Gray Values										
	0 s	10 s	20 s	30 s	40 s	50 s	60 s	70 s	80 s	90 s	100 s
7.416	25307	25196	25230	25223	25244	25244	25258	25244	25251	25251	25272
7.463	25327	25251	25300	25265	25327	25300	25327	25348	25334	25348	25369
7.509	25043	24960	25016	25016	25023	25057	25071	25092	25127	25134	25140
7.556	24641	24572	24593	24607	24621	24655	24683	24697	24711	24745	24759
7.603	24191	24177	24191	24205	24205	24246	24267	24295	24295	24330	24323
7.649	23893	23831	23789	23817	23824	23845	23824	23872	23893	23921	23914
7.696	23789	23768	23713	23720	23713	23685	23685	23699	23713	23727	23761
7.743	23803	23775	23810	23845	23858	23858	23824	23831	23803	23824	23831
7.789	23755	23734	23762	23727	23741	23803	23803	23782	23768	23775	23775
7.836	23630	23685	23678	23637	23630	23685	23678	23692	23651	23665	23678
7.882	23443	23464	23491	23457	23450	23485	23471	23464	23471	23478	23505
7.929	23464	23519	23554	23519	23485	23519	23492	23471	23491	23491	23526
7.976	23471	23429	23457	23436	23415	23436	23436	23388	23415	23415	23429
8.022	23595	23526	23512	23526	23519	23505	23519	23505	23512	23505	23505
8.069	23388	23367	23374	23360	23353	23325	23353	23360	23395	23388	23381
8.116	23381	23450	23415	23450	23450	23443	23457	23443	23443	23450	23457
8.162	23304	23422	23374	23401	23367	23360	23381	23388	23360	23360	23374
8.209	23332	23450	23429	23422	23367	23381	23388	23360	23367	23374	23374
8.256	23415	23498	23429	23415	23401	23388	23381	23381	23395	23381	23374
8.302	23602	23630	23588	23554	23547	23526	23505	23505	23519	23512	23498
8.349	23325	23346	23284	23284	23298	23270	23256	23298	23304	23277	23277
8.396	23221	23291	23242	23284	23304	23270	23242	23263	23263	23263	23249
8.442	23117	23194	23152	23201	23214	23208	23214	23201	23221	23194	23208
8.489	23173	23235	23242	23228	23270	23305	23242	23249	23242	23214	23249
8.535	23173	23194	23208	23214	23270	23235	23221	23214	23228	23228	23214
8.582	23318	23235	23242	23284	23291	23263	23263	23284	23277	23256	23270
8.629	23304	23256	23214	23207	23207	23194	23214	23228	23207	23200	23207
8.675	23242	23228	23228	23207	23214	23221	23228	23221	23200	23235	23228
8.722	23277	23346	23318	23318	23318	23325	23325	23311	23318	23311	23311
8.769	23325	23374	23381	23353	23318	23325	23325	23332	23325	23318	23318
8.815	23304	23305	23291	23263	23256	23263	23214	23208	23214	23214	23208
8.862	23291	23277	23235	23214	23187	23187	23194	23201	23180	23180	23173
8.909	23422	23436	23429	23415	23388	23388	23374	23367	23332	23346	23353
8.955	23346	23360	23360	23367	23332	23346	23346	23339	23291	23298	23291
9.002	23284	23256	23263	23228	23249	23256	23249	23242	23242	23256	23270
9.049	23436	23388	23374	23311	23311	23318	23284	23284	23284	23277	23284
9.095	23408	23325	23367	23298	23298	23325	23298	23305	23318	23304	23311
9.142	23346	23305	23291	23270	23277	23270	23263	23256	23270	23291	23277
9.188	23221	23214	23194	23228	23214	23207	23214	23242	23242	23214	23221
9.235	23090	23083	23083	23104	23111	23090	23104	23104	23131	23131	23138
9.282	23117	23145	23152	23194	23194	23180	23166	23187	23194	23180	23194
9.328	23138	23117	23131	23194	23208	23159	23180	23145	23138	23131	23145

Position (mm)	Gray Values										
	0 s	10 s	20 s	30 s	40 s	50 s	60 s	70 s	80 s	90 s	100 s
9.375	23318	23228	23166	23201	23214	23166	23166	23173	23145	23152	23173
9.422	23374	23242	23201	23180	23180	23131	23104	23117	23111	23117	23138
9.468	23263	23104	23097	23055	23069	23069	23055	23055	23069	23062	23090
9.515	23298	23124	23131	23110	23090	23097	23090	23083	23090	23090	23104
9.562	23388	23235	23208	23187	23187	23187	23221	23208	23208	23207	23221
9.608	23152	23090	23104	23090	23117	23138	23131	23145	23152	23145	23131
9.655	22972	22972	23041	23020	23034	23062	23076	23069	23069	23104	23097
9.701	22889	22965	22993	23014	23062	23014	23069	23062	23076	23104	23104
9.748	22972	23041	23027	23062	23090	23090	23090	23090	23097	23097	23069
9.795	22958	22972	22937	22986	22986	22986	22986	22993	22993	22993	22986
9.841	23180	23124	23124	23131	23138	23124	23124	23131	23131	23152	23124
9.888	23076	23069	23020	23097	23124	23090	23097	23117	23097	23131	23131
9.935	23055	23069	23055	23076	23097	23083	23069	23117	23111	23111	23111
9.981	23110	23090	23124	23097	23097	23117	23117	23124	23138	23138	23131
10.028	23325	23270	23298	23298	23284	23298	23291	23298	23291	23277	23284
10.075	23346	23311	23270	23284	23242	23277	23221	23228	23207	23235	23235
10.121	23270	23360	23249	23291	23221	23249	23235	23242	23249	23242	23249
10.168	23145	23166	23117	23152	23110	23104	23117	23117	23124	23138	23131
10.215	23200	23152	23145	23152	23159	23166	23159	23180	23180	23131	23166
10.261	23207	23131	23110	23124	23138	23145	23131	23131	23131	23110	23117
10.308	23159	23138	23117	23111	23138	23187	23145	23159	23159	23166	23159
10.354	23083	23083	23111	23104	23131	23138	23117	23117	23117	23117	23131
10.401	23270	23256	23270	23256	23270	23256	23256	23256	23249	23249	23242
10.448	23228	23145	23117	23097	23131	23138	23138	23131	23131	23131	23138
10.494	23117	23069	23103	23110	23138	23131	23145	23145	23152	23152	23145
10.541	22916	23027	23034	23041	23083	23097	23097	23110	23104	23104	23117
10.588	23110	23200	23200	23173	23201	23221	23235	23214	23194	23235	23228
10.634	22972	22972	22965	22930	22937	22937	22923	22923	22923	22923	22944
10.681	23242	23221	23194	23166	23152	23138	23152	23111	23166	23159	23166
10.728	23083	23111	23048	23069	23076	23069	23041	23041	23048	23048	23055
10.774	23097	23104	23062	23076	23034	23055	23062	23062	23083	23062	23069
10.821	23055	23124	23055	23006	23027	23006	23034	23034	23027	23048	23034
10.868	23166	23117	23076	23076	23097	23103	23145	23131	23159	23166	23145
10.914	23117	23027	23020	23048	23041	23048	23062	23048	23048	23083	23076
10.961	23291	23173	23131	23145	23131	23138	23110	23117	23124	23097	23131
11.007	23090	23034	22965	22993	23013	22986	22979	22979	22972	22993	22986
11.054	23221	23138	23152	23159	23152	23145	23124	23131	23152	23152	23152
11.101	23069	23048	23104	23124	23131	23110	23104	23117	23124	23117	23110
11.147	23374	23297	23346	23325	23332	23311	23318	23318	23298	23311	23304
11.194	23124	23083	23076	23055	23083	23069	23069	23062	23055	23034	23034
11.241	23138	23152	23117	23145	23159	23173	23173	23152	23159	23152	23159
11.287	23020	23020	23027	23027	23041	23062	23062	23069	23069	23076	23055

Position (mm)	Gray Values										
	0 s	10 s	20 s	30 s	40 s	50 s	60 s	70 s	80 s	90 s	100 s
11.334	23256	23159	23152	23145	23110	23131	23159	23152	23152	23152	23152
11.381	23152	23145	23117	23104	23117	23097	23117	23124	23138	23117	23124
11.427	23180	23187	23194	23214	23214	23194	23214	23201	23214	23187	23201
11.474	22826	22944	23048	23034	23055	23027	23020	23027	23013	23020	23007
11.521	22889	23014	23090	23097	23069	23083	23097	23076	23069	23076	23083
11.567	22903	22944	22958	22958	22972	22972	23007	23000	22986	22965	22972
11.614	23187	23173	23145	23117	23138	23152	23173	23173	23152	23180	23173
11.660	23090	23034	23007	22986	22965	23013	23013	23034	23020	23034	23034
11.707	23235	23083	23097	23110	23090	23124	23117	23145	23124	23090	23090
11.754	23131	22993	23000	23000	23000	22972	22986	22986	22979	22951	22958
11.800	23291	23228	23256	23200	23228	23221	23214	23214	23214	23201	23180
11.847	23000	23069	23117	23055	23110	23104	23090	23097	23069	23083	23083
11.894	22951	23013	23041	23000	23007	23007	23000	23007	23007	23013	23034
11.940	22910	22847	22868	22875	22861	22889	22875	22910	22923	22937	22917
11.987	22993	22916	22861	22889	22840	22903	22896	22909	22923	22923	22916
12.034	23069	22986	22958	22916	22951	22972	22944	22958	22965	22951	22979
12.080	23076	23041	23007	23013	23027	23048	23055	23041	23048	23041	23027
12.127	22951	22882	22889	22910	22896	22896	22910	22903	22910	22916	22923
12.174	23103	23104	23097	23090	23090	23097	23097	23090	23104	23110	23110
12.220	23000	23055	23007	23020	23007	23020	23007	23013	23027	23034	23027
12.267	22993	23013	22986	22972	22965	23007	22993	22979	22986	23007	22986
12.313	22896	22965	22965	22903	22896	22937	22951	22951	22944	22951	22937
12.360	22944	22958	22972	22903	22916	22930	22923	22944	22937	22930	22923
12.407	22889	22861	22882	22875	22861	22868	22889	22861	22868	22875	22889
12.453	23014	22937	22944	22916	22903	22916	22875	22910	22923	22896	22916
12.500	23034	22930	22923	22916	22937	22937	22930	22937	22937	22944	22944
12.547	23020	23020	23007	23027	23055	23048	23055	23097	23076	23076	23083
12.593	22993	22958	22951	23000	23007	22972	22979	22993	23007	23007	23020
12.640	22972	22889	22916	22889	22910	22882	22868	22896	22868	22868	22868
12.687	22909	22833	22854	22840	22812	22806	22799	22785	22771	22771	22771
12.733	22806	22750	22812	22764	22778	22792	22785	22778	22764	22757	22750
12.780	22715	22736	22806	22771	22785	22785	22792	22785	22792	22799	22785
12.826	22868	22868	22896	22889	22875	22882	22861	22882	22882	22854	22861
12.873	22875	22889	22854	22840	22806	22819	22819	22840	22833	22819	22833
12.920	22757	22778	22681	22688	22695	22674	22681	22688	22681	22695	22681
12.966	22688	22757	22750	22729	22757	22764	22729	22750	22778	22778	22778
13.013	22868	22923	22930	22923	22910	22937	22910	22903	22923	22910	22910
13.060	22806	22861	22889	22896	22889	22896	22896	22882	22875	22875	22868
13.106	22826	22868	22861	22875	22854	22840	22847	22868	22896	22889	22868
13.153	22826	22868	22896	22916	22868	22861	22875	22882	22882	22910	22882
13.200	22826	22847	22861	22861	22840	22813	22826	22847	22868	22896	22882
13.246	23117	23041	23020	23034	22993	23000	23020	23007	23020	23027	23013

Position (mm)	Gray Values										
	0 s	10 s	20 s	30 s	40 s	50 s	60 s	70 s	80 s	90 s	100 s
13.293	22951	22937	22930	22930	22882	22916	22909	22909	22896	22896	22889
13.340	22903	22937	22958	22937	22910	22937	22916	22944	22951	22937	22903
13.386	22743	22944	22889	22896	22889	22930	22916	22916	22916	22910	22889
13.433	22632	22764	22819	22819	22799	22819	22806	22806	22778	22778	22785
13.479	22709	22743	22757	22799	22722	22715	22729	22702	22716	22702	22715
13.526	22854	22937	22916	22903	22847	22847	22840	22819	22833	22819	22826
13.573	22993	23007	22986	22937	22923	22896	22889	22875	22868	22861	22861
13.619	22916	22951	22882	22861	22882	22847	22854	22854	22826	22826	22826
13.666	22757	22792	22785	22771	22757	22743	22736	22743	22736	22750	22729
13.713	22903	22819	22910	22937	22923	22903	22875	22847	22861	22868	22889
13.759	22882	22771	22806	22833	22840	22826	22819	22826	22826	22833	22833
13.806	22930	22937	22965	22965	22937	22923	22951	22937	22909	22896	22896
13.853	22716	22729	22702	22722	22722	22729	22764	22743	22743	22743	22716
13.899	22757	22847	22819	22854	22875	22889	22896	22930	22889	22868	22882
13.946	22521	22646	22605	22612	22584	22612	22653	22653	22639	22639	22612
13.993	22556	22702	22639	22646	22632	22674	22681	22681	22695	22688	22702
14.039	22605	22667	22598	22625	22598	22639	22632	22667	22688	22688	22674
14.086	22771	22778	22729	22729	22764	22750	22778	22799	22799	22771	22764
14.132	22688	22722	22688	22660	22653	22688	22702	22688	22722	22729	22715
14.179	22813	22875	22833	22854	22819	22847	22833	22847	22868	22875	22875
14.226	22619	22584	22584	22563	22542	22570	22577	22598	22598	22584	22570
14.272	22840	22764	22709	22722	22702	22715	22709	22715	22709	22695	22681
14.319	22653	22577	22521	22528	22542	22549	22528	22563	22570	22570	22563
14.366	22743	22736	22722	22722	22743	22729	22736	22743	22750	22764	22743
14.412	22646	22625	22618	22632	22660	22660	22660	22688	22688	22695	22688
14.459	22639	22653	22646	22674	22674	22688	22702	22709	22688	22709	22709
14.506	22501	22515	22521	22528	22521	22528	22563	22549	22528	22535	22535
14.552	22695	22729	22688	22674	22632	22653	22667	22674	22667	22667	22681
14.599	22598	22639	22653	22612	22570	22618	22612	22612	22605	22598	22625
14.646	22840	22819	22799	22785	22785	22771	22792	22785	22764	22736	22736
14.692	22833	22702	22709	22695	22667	22695	22674	22674	22674	22667	22674
14.739	22847	22785	22792	22736	22757	22750	22778	22792	22757	22757	22757
14.785	22750	22709	22722	22722	22674	22639	22674	22660	22653	22646	22653
14.832	22750	22819	22813	22799	22771	22757	22750	22757	22743	22750	22750
14.879	22660	22715	22722	22695	22653	22639	22625	22653	22653	22653	22639
14.925	22667	22702	22709	22709	22660	22625	22632	22632	22653	22653	22653
14.972	22480	22542	22549	22563	22508	22508	22535	22535	22542	22535	22549
15.019	22660	22702	22660	22688	22667	22667	22667	22667	22681	22702	22681
15.065	22535	22542	22521	22508	22508	22521	22549	22549	22563	22563	22556

Table C-2. Interface displacement in 1000 seconds with 10 seconds time intervals.

Time (s)	Position (mm)								
10	7.621	210	7.688	410	7.770	610	7.824	810	7.847
20	7.617	220	7.692	420	7.772	620	7.829	820	7.847
30	7.616	230	7.693	430	7.771	630	7.828	830	7.847
40	7.619	240	7.694	440	7.771	640	7.828	840	7.847
50	7.619	250	7.695	450	7.773	650	7.830	850	7.849
60	7.623	260	7.701	460	7.805	660	7.826	860	7.850
70	7.623	270	7.698	470	7.811	670	7.827	870	7.849
80	7.627	280	7.706	480	7.801	680	7.828	880	7.850
90	7.628	290	7.709	490	7.802	690	7.829	890	7.850
100	7.632	300	7.711	500	7.806	700	7.828	900	7.850
110	7.631	310	7.765	510	7.803	710	7.830	910	7.864
120	7.635	320	7.770	520	7.803	720	7.830	920	7.861
130	7.639	330	7.769	530	7.807	730	7.829	930	7.865
140	7.642	340	7.763	540	7.810	740	7.829	940	7.865
150	7.643	350	7.767	550	7.809	750	7.832	950	7.865
160	7.670	360	7.764	560	7.809	760	7.843	960	7.867
170	7.674	370	7.766	570	7.812	770	7.845	970	7.866
180	7.676	380	7.766	580	7.811	780	7.847	980	7.867
190	7.680	390	7.767	590	7.811	790	7.845	990	7.866
200	7.682	400	7.768	600	7.812	800	7.846	1000	7.866

Table C-3. Interface displacement from 250 to 350 seconds with 0.5 seconds time intervals.

Time (s)	Position (mm)								
250.0	7.711	270.0	7.714	290.0	7.720	310.0	7.752	330.0	7.754
250.5	7.710	270.5	7.715	290.5	7.720	310.5	7.754	330.5	7.757
251.0	7.709	271.0	7.714	291.0	7.720	311.0	7.753	331.0	7.757
251.5	7.709	271.5	7.714	291.5	7.720	311.5	7.754	331.5	7.758
252.0	7.709	272.0	7.714	292.0	7.720	312.0	7.752	332.0	7.757
252.5	7.709	272.5	7.715	292.5	7.720	312.5	7.753	332.5	7.758
253.0	7.709	273.0	7.715	293.0	7.720	313.0	7.752	333.0	7.758
253.5	7.709	273.5	7.716	293.5	7.720	313.5	7.753	333.5	7.758
254.0	7.709	274.0	7.716	294.0	7.720	314.0	7.752	334.0	7.758
254.5	7.709	274.5	7.716	294.5	7.720	314.5	7.751	334.5	7.759
255.0	7.710	275.0	7.716	295.0	7.720	315.0	7.752	335.0	7.759
255.5	7.709	275.5	7.716	295.5	7.720	315.5	7.754	335.5	7.759
256.0	7.709	276.0	7.716	296.0	7.721	316.0	7.753	336.0	7.759
256.5	7.709	276.5	7.716	296.5	7.721	316.5	7.754	336.5	7.758
257.0	7.710	277.0	7.716	297.0	7.721	317.0	7.753	337.0	7.759
257.5	7.709	277.5	7.716	297.5	7.720	317.5	7.754	337.5	7.759
258.0	7.710	278.0	7.717	298.0	7.720	318.0	7.756	338.0	7.760
258.5	7.709	278.5	7.717	298.5	7.721	318.5	7.755	338.5	7.760
259.0	7.709	279.0	7.717	299.0	7.722	319.0	7.756	339.0	7.760
259.5	7.710	279.5	7.718	299.5	7.722	319.5	7.754	339.5	7.759
260.0	7.710	280.0	7.718	300.0	7.722	320.0	7.755	340.0	7.760
260.5	7.710	280.5	7.718	300.5	7.722	320.5	7.756	340.5	7.760
261.0	7.711	281.0	7.718	301.0	7.724	321.0	7.755	341.0	7.761
261.5	7.711	281.5	7.718	301.5	7.725	321.5	7.755	341.5	7.758
262.0	7.710	282.0	7.718	302.0	7.724	322.0	7.755	342.0	7.757
262.5	7.712	282.5	7.718	302.5	7.731	322.5	7.754	342.5	7.758
263.0	7.712	283.0	7.718	303.0	7.736	323.0	7.754	343.0	7.758
263.5	7.711	283.5	7.718	303.5	7.740	323.5	7.754	343.5	7.758
264.0	7.712	284.0	7.718	304.0	7.745	324.0	7.757	344.0	7.759
264.5	7.712	284.5	7.718	304.5	7.739	324.5	7.755	344.5	7.759
265.0	7.712	285.0	7.719	305.0	7.745	325.0	7.754	345.0	7.760
265.5	7.713	285.5	7.718	305.5	7.748	325.5	7.756	345.5	7.759
266.0	7.712	286.0	7.718	306.0	7.753	326.0	7.755	346.0	7.759
266.5	7.712	286.5	7.718	306.5	7.753	326.5	7.755	346.5	7.761
267.0	7.713	287.0	7.718	307.0	7.753	327.0	7.754	347.0	7.761
267.5	7.712	287.5	7.720	307.5	7.754	327.5	7.754	347.5	7.760
268.0	7.712	288.0	7.720	308.0	7.754	328.0	7.754	348.0	7.759
268.5	7.712	288.5	7.720	308.5	7.756	328.5	7.756	348.5	7.760
269.0	7.713	289.0	7.720	309.0	7.753	329.0	7.756	349.0	7.760
269.5	7.713	289.5	7.720	309.5	7.752	329.5	7.755	349.5	7.761